Second Harmonic Generation Microscopy of Inner Ear Otoconia

By
Kennedy Brittain

A Thesis Submitted to
Saint Mary's University, Halifax, Nova Scotia
in Partial Fulfillment of the Requirements for
the Degree of Bachelor of Science – Honours Biology

April 2020, Halifax, Nova Scotia

Approved: Dr. Danielle Tokarz

_____
Supervisor

Approved: Dr. Ron Russel

_____
Thesis Reader

Date: May 1st, 2020

Second Harmonic Generation Microscopy of Inner Ear Otoconia

By: Kennedy Brittain

ABSTRACT

Otoconia are microscopic biocrystals located within the vestibular system of the inner ear, that allow vertebrates to detect gravity and linear acceleration. When otoconia become degraded due to factors including aging, disease, and consumption of ototoxic medications, vestibular pathologies arise, and the body's ability to maintain balance is significantly impaired. Vestibular pathologies such as benign-paroxysmal positional vertigo are a significant health concern across Canada. These pathologies lead to falls which cause debilitating conditions such as bone fractures, neurological damage, and negative social impacts. To develop methods to prevent degeneration of otoconia, and to induce and promote repair and regeneration, it is important to study their crystalline ultrastructure. In this study, we investigate the origin of second harmonic generation (SHG) signal in otoconia and their internal structural properties using SHG microscopy. SHG microscopy allows for optical sectioning of otoconia providing a 3D image of them, unlike previously used imaging techniques. To determine the origin of SHG signal of otoconia, calcite, the principal component of otoconia (>90 wt. -%) was imaged using SHG microscopy. Calcite gave ~41× less SHG signal compared to otoconia. Therefore, it was determined that calcite is unlikely the origin of SHG signal in otoconia. This finding indicates that proteins in otoconia are likely causing the SHG signal in otoconia as they make up the remaining portion of otoconia (<5 wt. -%). SHG images of otoconia revealed that they are polarization-dependent. This indicates that the proteins emitting SHG in otoconia are radially arranged, extending from a central region. Otoconia were also imaged after exposure to 0.5M ethylenediaminetetraacetic acid (EDTA), which degrades calcium carbonate. SHG signal increased over time, further supporting that proteins are causing the SHG signal in otoconia. It was concluded that SHG microscopy is a promising technique for investigating the internal structural properties of otoconia.

Acknowledgements

I would firstly like to thank my supervisors Dr. Danielle Tokarz and Dr. Richard Cisek for providing me the opportunity to perform my honours research project with them. I would also like to thank them for their continued support and guidance throughout the duration of this project. Furthermore, I would like to thank the members of the Tokarz research group: Ariana Joseph, Katherine Purvis, and Macaulay Harvey. While working with the Tokarz research group I have learned to always question the facts, to remain curious, and to persevere through failure (or even several failures). In addition, I would like to thank Dr. Sean Christie and Dr. Saranyan Pillai from the Brain Repair Centre at Dalhousie University for providing me with mice specimens and for giving continuous guidance throughout the dissection process of this experiment. Additionally, I would like to thank Dr. Jacob Hanley and Dr. Mitchell Kerr for generously donating the calcite samples used throughout this experiment. I would also like to thank Dr. Colleen Barber for her kind words of encouragement while completing this project. Lastly, I would like to thank my family, friends, and the honours thesis class of 2020 for always pushing me forward and supporting me along the way.

Table of Contents

Abstract..... 2
Acknowledgements..... 3
Table of Contents..... 4
List of Figures..... 5
List of Tables..... 6

1. INTRODUCTION..... **7**

1.1 The Vestibular System..... 7
1.2 Otoconia Function..... 9
1.3 Vestibular Pathologies..... 10
1.4 Otoconia Structure..... 12
1.5 Otoconia Development..... 14
1.6 Ototoxic Medications..... 15
1.7 Second Harmonic Generation Microscopy..... 16
1.8 Study Objectives..... 18

2. MATERIALS AND METHODS..... **20**

2.1 Methods Summary..... 20
2.2 Temporal Bone Isolation..... 20
2.3 Otoconia Isolation..... 22
2.4 Second Harmonic Generation Microscopy..... 23
2.5 Calcite..... 24
2.6 Otoconia and Calcite Degradation Experiments..... 26
2.7 Analysis Methods..... 27

3. RESULTS..... **29**

3.1 Calcite Mineral SHG Imaging...... 29
3.2 Purified Calcite SHG Imaging..... 32
3.3 Calcite EDTA Degradation Over Time..... 34
3.4 Otoconia SHG Imaging..... 35
3.5 Otoconia EDTA Degradation Over Time..... 38

4. DISCUSSION..... **45**

4.1 Study Objective 1: Determine the Origin of SHG signal in Otoconia..... 45
4.2 Study Objective 2: Determine the internal structural properties of otoconia and the changes that occur during degradation using SHG microscopy..... 47
4.3 Future Research and Applications..... 49

LITERATURE CITED..... **51**

List of Figures

Figure 1. A model depicting the five primary structures of the vestibular system..... 1
Figure 2. Current 3D model of the internal structure of mammalian otoconia…….... 14
Figure 3. Energy State Diagrams of single photon excitation fluorescence (SPF) and second harmonic generation (SHG)…….……..... 18
Figure 4. The temporal bone of the common house mouse (*mus musculus*), before removal of the utricle……..... 23
Figure 5. A schematic of the home-built non-linear optical microscope set-up used to acquire SHG images…….…..... 24
Figure 6. Second Harmonic Generation microscopy images of calcite mineral in 0.1M sodium cacodylate buffer (pH 7.4)..... 29
Figure 7. SHG microscopy images of calcite mineral in acrylamide gel and 0.1M sodium cacodylate buffer (pH 7.4)..... 31
Figure 8. Purified calcite crystals imaged using Second harmonic generation microscopy and Third harmonic generation microscopy..... 33
Figure 9. SHG microscopy images of pure calcite crystals grown to a larger particle size..... 33
Figure 10. Calcite mineral in 0.5M EDTA imaged using SHG microscopy over a period of 90 minutes..... 34
Figure 11. The mean SHG intensity of calcite mineral in 0.5M EDTA over a period of 90 minutes..... 35
Figure 12. Otoconia imaged using SHG at two different linear laser polarizations..... 36
Figure 13. A single otoconium imaged using SHG microscopy at eight polarization angles..... 37
Figure 14. Otoconia imaged with SHG microscopy using circularly polarized light..... 38
Figure 15. Plot of mean SHG intensity of otoconia #1 over time after exposure to 0.5M EDTA..... 39
Figure 16. Otoconia #1 imaged after exposure to 0.5M EDTA at the beginning of the experiment and end of the experiment..... 40
Figure 17. Plot of mean SHG intensity of otoconia #2 over time after exposure to 0.5M EDTA..... 41
Figure 18. Otoconia #2 imaged after exposure to 0.5M EDTA at the beginning of the experiment and end of the experiment..... 42
Figure 19. Plot of mean SHG intensity of otoconia #3 over time after exposure to 0.5M EDTA..... 43
Figure 20. Otoconia #3 imaged after exposure to 0.5M EDTA at the beginning of the experiment and end of the experiment..... 44
Figure 21. A model of the hypothesized arrangement of proteins causing the SHG signal in otoconia..... 48

List of Tables

Table 1. The standardized SHG intensities of calcite mineral imaged in 0.1M sodium cacodylate buffer.....30

Table 2. Mean SHG Intensities for calcite mineral imaged with acrylamide gel and 0.1M sodium cacodylate buffer (pH 7.4).....32

1. INTRODUCTION

1.1 The Vestibular System

The vestibular system is classified as a sensory system and therefore functions to translate environmental stimuli into biological signals (Baloh et al. 2011). The specific functions of this system are to maintain spatial orientation and stabilize vision and balance (Baloh et al. 2011). The vestibular system is located within the inner ear and consists of five primary structures. These structures shown in Figure 1 include the anterior, posterior, and horizontal semicircular canals (all approximately 90° apart), and two otolith organs, the utricle and saccule (Agrawal et al. 2012).

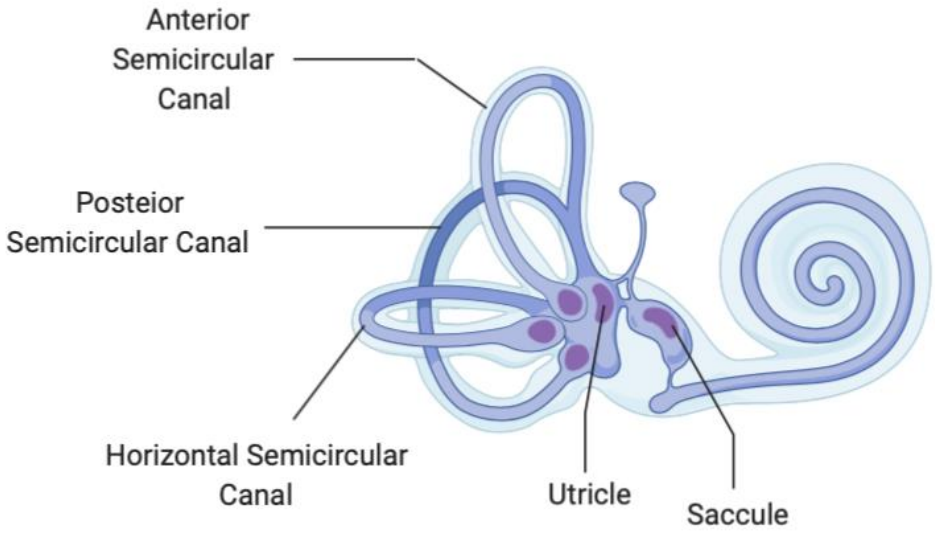

Figure 1: A schematic of the vestibular system of the inner ear. The vestibular system detects motions of the head, allowing vertebrates to maintain balance (Casale and Gupta 2019). This image was modified using BioRender.

The semicircular canals located within the bony labyrinth of the inner ear function to detect rotational movements of the head. Each of the semicircular canals consists of an

expansion known as the ampulla, which houses a sensory epithelium called the crista (Rabbitt 2019). The crista contains stereocilia, which are hair-like cells that extend into a gelatinous mass called the cupula (Rabbitt 2019). Due to its gel-like composition, the cupula is highly flexible and becomes distorted by force produced by the movement of external endolymph, which is the major fluid component found in the inner ear (Purves et al. 2001). The distortion of the cupula causes the stereocilia within it to be displaced, allowing for the detection of rotational acceleration through axon activation (Purves et al. 2001).

Unlike the semicircular canals, the otolithic organs detect linear movements rather than rotational (Christopher and Rosenberg 2018). The saccule, one of the two otolithic organs, is globular and smaller in shape compared to the oblong utricle (Okeke et al. 2016). The saccule and utricle are not directly connected, but remain linked through ducts that lead to the endolymphatic sac, which stores endolymph and removes any excess fluid that may be present within the inner ear (Brauer 2003). The ionic composition of the endolymph is highly regulated to ensure that the depolarization of hair cells caused by movements can occur as efficiently as possible (Hopkins 2015). The main ionic component of this fluid is potassium, and it acts as the depolarizing agent in this region of the inner ear (Fettiplace 2017). The high concentration of potassium in the endolymph is regulated by sodium/potassium ATPase's, located on dark cells in the cristae of the semicircular canals (Casale and Agarwal 2019). Together these structures allow the body to perceive gravity and adjust its movements and posture to maintain balance and orientation (Glover 2004).

1.2 Otoconia Function

The otolithic organs: the utricle and the saccule, are two complementary organs found in the vestibule of the inner ear that allow for the detection of gravity and linear acceleration, respectively (Dakin and Rosenberg 2018). In particular, the saccule detects acceleration along a vertical axis in addition to detecting gravity, while the utricle detects horizontal acceleration (Casale and Gupta 2019). Both organs consist of a sensory epithelium called the macula, which contains bundles of stereocilia. Similarly to those found in the semicircular canals, they detect and respond to mechanical stimuli (Lundberg et al. 2015). The macula of the utricle is horizontally oriented, whereas the saccule macula is more vertical (Purves et al. 2001).

Above the stereocilia lies a gel-like layer called the cupula, similar to the one found in the semicircular canals. The cupula is found just below the otolithic membrane, which houses approximately 200 000 small biocrystals, called otoconia (Mason 2017). Due to the large mass of these otoconia relative to the other nearby structures and fluids, when a person's head moves, their membrane becomes displaced as well (Purves et al. 2001). When the body is in motion, the stereocilia are either bent towards or away from a structure known as a kinocilium. The kinocilium is the longest cilium in each of every hair-like cell bundle and is surrounded by approximately 40-70 stereocilia (Casale and Gupta 2019).

The displacement of this bundle caused by a shift in the otolithic membrane causes the potassium channels of the stereocilia to open when they are shifted towards the kinocilium (Lundberg et al. 2015). This event leads to depolarization of the stereocilia and opening of voltage-gated calcium channels allowing signals to be sent to the central

nervous system through the afferent vestibular nerve (Lundberg et al. 2015). If the stereocilia are shifted away from the kinocilium, the cells will hyperpolarize. As a result, firing rates will be reduced compared to when there is no motion, and the stereocilia remain upright (Casale and Gupta 2019). These signals sent to the central nervous system or a reduction in firing rate, gives the body the information it requires to adjust its movements and posture in order to maintain balance and stabilize vision (Barral et al. 2009).

1.3 Vestibular Pathologies

Vestibular pathologies are a significant health concern across Canada and the world but are especially detrimental to our senior population. Loss of coordination and balance leading to falls causes several debilitating conditions such as bone fractures, neurological damage, and can have lasting negative social impacts on seniors who fear they may fall again (Fasano and Plotnik 2012). Falls due to vestibular-related disorders lead to increased hospitalization rates and wait times, which is especially detrimental in provinces such as Nova Scotia, where the health care system is already strained (Watson et al. 2015) (Wilson and Rosenberg 2002). In Nova Scotia alone, 61% of injury-related hospital admissions are due to the result of seniors falling (Nova Scotia Health Promotion and Protection 2007). In addition to the strain that these falls place on our health care system, they also place a substantial economic burden on the province as well. Data from 1999 showed that falls cost Nova Scotians 72 million dollars per year alone (Atlantic Network for Injury Prevention 2003).

Benign paroxysmal positional vertigo (BPPV) is the leading cause of vestibular malfunction. It is, therefore, one of the most significant contributors to dizziness and imbalance in the elderly (Iwasaki and Yamasoba 2015). BPPV is a debilitating condition that causes symptoms such as dizziness, nausea, and a sense that one's surroundings are in motion (Parnes et al. 2003). It is currently thought that BPPV is caused by canalithiasis. Canalithiasis is the phenomenon that occurs when otoconia, or pieces of otoconia, become dislodged from the utricle and saccule and are trapped within the semicircular canals (Parnes et al. 2003).

There are three leading causes of BPPV, including head trauma, infection, and degeneration of otoconia (Johnson 2009). Firstly, when an individual suffers a forceful injury to the head, it can cause the otoconia to become released from their membrane into the endolymph, where they make their way to the semicircular canals (Johnson 2009). There is also evidence that there is a link between viral infections and BPPV, although the exact mechanisms are unknown (Hancı et al. 2015) Lastly, BPPV can also occur as a result of otoconia degeneration (Hain 2007).

Otoconia degeneration can be caused by several factors, including aging, disease, and consumption of ototoxic medications (Palmeri and Kumar 2019). This degeneration on its own can lead to dizziness and imbalance as it alters the mass of the otoconia leading to poor perception of gravity. This impairs the body's ability to adjust its movements and posture correctly (Hughes et al. 2006). In addition, this degeneration leads to pieces of fragmented otoconia, making their way to the semicircular canals (Kao et al. 2017). Since otoconia are not regenerated, current therapies have limited effect and are only able to treat

symptoms temporarily. The mechanism of how otoconia degenerate and become dislodged is currently unknown and requires further investigation (Walther et al. 2014).

1.4 Otoconia Structure

Mammalian otoconia have a barrel-shaped body that ends in three rhombohedral faces that join at a point on each end (Lins et al. 2000). Current research shows that the inner structure of otoconia is comprised of three dense branches extending from a central point towards each of the two ends (Kniep et al. 2017). This dense region is surrounded by a porous and more vulnerable belly region due to a disorganized nanocomposite crystal organization (Figure 2) (Kniep et al. 2017). The branched region of the otoconia is denser due to a more ordered nanocomposite crystal pattern, which is strengthened further by parallel fibers made of proteins that run adjacent to the densely packed crystal units (Walther et al. 2014). This is different from the previous assumption that otoconia had an inner core from which crystal growth would occur (Walther et al. 2014).

Otoconia can vary in length, but the mean length of human otoconia is ~10 μm (Walther et al. 2014). Otoconia are primarily composed of calcium carbonate crystal in the polymorphic form of calcite (Lim 1973). In addition to their crystallinity, mammalian otoconia are composed of an organic matrix of proteins that is embedded within the otoconium and continues to extend outwards from their surface as fibrils, which help to join neighbouring otoconia together (Kourosh 2014). The organic fraction of the otoconia only represents a small portion of their mass (<5 wt. -%) compared to its calcite composition (>90 wt. -%) (Walther et al. 2014). The organic fraction consists mainly of glycoproteins and glycosaminoglycans (Walther et al. 2014). The most abundant soluble

protein (>90%) within the crystals is otoconin-90. Otoconin-90 is a glycoprotein that is thought to function in collecting and assembling the necessary components for the development of the remaining organic matrix (Hughes et al. 2006). This in turn helps direct the morphology of otoconia (Hughes et al. 2006) (Lu et al. 2010). Another essential protein in otoconia development is otolin, which is structurally and chemically similar to collagen and makes up part of the fibrils that help anchor and join otoconia together (Murayama et al. 2005).

Otoconia have a 3-fold rotation axis and a center of symmetry making them an overall centrosymmetric structure with a symmetry point group close to -3m (Kniep et al. 2017). However, recent research suggests that the overall symmetry of these crystals may not be as close to -3m as previously thought due to uneven size observations of their rhombohedral faces (Kniep et al. 2017). To investigate the structural properties of otoconia, mice are commonly used as a model species due to their structural and compositional similarities to humans along with analogous mechanisms of otoconia formation (Hughes et al. 2006). Despite recent advancements, there is still limited and conflicting information regarding the internal structural properties of otoconia such as the crystal and protein arrangement (Walther et al. 2014).

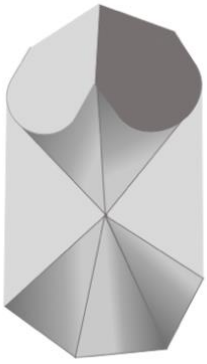

Figure 2: Diagram of the current proposed 3D model of the internal structure of mammalian otoconia. The crystals exhibit an approximate -3m crystal point symmetry and a dense 3+3 branching pattern extending from a central point towards the rhombohedral faces at each end of the otoconium. The belly-region of the otoconium is porous and less dense due to a disorganized nanocomposite crystalline structure. Figure modified from (Kniep et al. 2017).

1.5 Otoconia Development

Current research shows that the organic matrix of proteins located within the otoconia is most likely the causative agent of otoconia formation, along with additionally having roles in directing the shape and size of the crystals (Lundberg et al. 2015). Otoconin-90 has been found to be very closely related to a secretory enzyme called phospholipase A2 (sPLA2) (Wang et al. 1998). While otoconin-90 did not retain the enzyme's catalytic activity, it did keep the enzyme's ability to bind calcium due to the acidic amino acid side chains located within the active site (Yang et al. 2011). Due to its binding abilities, otoconin-90 begins the crystal seeding process by recruiting additional matrix proteins and sequestering calcium (Yang et al. 2011). Calcium is abundant in the endolymph near the otolithic membrane due to calmodulin-sensitive plasma membrane calcium ATPases (PMCA), that exchange H^+ for Ca^{2+} to ensure there is sufficient Ca^{2+} in the region for otoconia growth (Lundberg et al. 2015).

Carbonic anhydrase is also an essential component of otoconial development and is expressed in the macula of the otolithic organs (Hughes et al. 2006). Carbonic anhydrase provides carbonate in order to form the calcite crystal and helps to create an optimal pH environment for otoconia growth (Hughes et al. 2006). Seeding of otoconia typically begins at embryonic day 14.5 (E14.5) for humans, and the seeds consist of a calcium carbonate core surrounded by an organic matrix (Lundberg et al. 2015). Otolin is thought to then create a scaffold of collagen-like proteins so that the crystallites are deposited in the correct orientation to ensure the characteristic otoconia structure is maintained (Deans et al. 2010). During growth, the otoconia are anchored to the otoconial membrane and linked to the sensory epithelium that will later allow for the detection of mechanical stimuli (Kao et al. 2017). Growth of otoconia is complete approximately one-week post-parturition (Lundberg et al. 2015).

1.6 Ototoxic Medications

Ototoxicity is the occurrence of adverse side-effects caused by therapeutic drugs and other chemical agents, leading to impaired function of the cochlear and vestibular portions of the inner ear (Bisht and Bist 2011). Many effective prescription medications are known to cause ototoxicity, including aminoglycoside antibiotics, platinum-based chemotherapeutic drugs, loop diuretics, macrolide antibiotics, and antimalarial medications (Rybak and Ramkumar 2007).

Ototoxicity contributes to degeneration of otoconia leading to the development of pathologies such as BPPV. It is thought that the degeneration caused by ototoxicity leads to fragmented pieces of the damaged otoconia becoming trapped inside the semicircular

canals leading to the development of BPPV (Walther et al. 2014). There is also evidence that ototoxicity and otoconia degeneration leads to weakening of the protein filaments that anchor otoconia to their membrane, further increasing the likelihood of developing BPPV (Kao et al. 2017). The development of vestibular pathologies from ototoxicity may occur quickly or slowly over time and is irreversible once the otoconia are damaged (Cianfrone et al. 2011).

Degeneration of otoconia due to ototoxicity has been observed using scanning electron microscopy (SEM) in previous studies (Walther et al. 2014). Information using SEM imaging reveals that minor degeneration is characterized by a rough surface and fissures on the belly region of the otoconia along with a slight reduction of calcite material (Walther et al. 2014). More severe degeneration is characterized by fractures along the otoconia, and significant degeneration of calcite material (Walther et al. 2014). The porous and more vulnerable belly region of otoconia is disintegrated first, and the denser branches of the rhombohedral faces are last (Walther et al. 2014). There is very limited information regarding the mechanism of how ototoxic drugs act to degrade otoconia and therefore, should be further investigated in order to develop suitable treatments (Pearson et al. 2019).

1.7 Second Harmonic Generation Microscopy

Second harmonic generation (SHG) microscopy is a valuable *in vivo* biological imaging technique that allows for longer duration scans compared to other common processes such as fluorescence, due to its ability to reduce photobleaching and photodamage (Mohler et al. 2003). The first observation of SHG occurred in 1961 when Franken, Hill, Peters, and Weinreich observed that light with twice the frequency of its

incident beam was detected when a ruby laser was focused into crystalline quartz (Franken et al. 1961). Since this observation, the development of SHG microscopy has been used to image numerous biological structures such as collagen (Mostaço-Guidolin et al. 2017), plant starch granules (Cisek et al. 2017), and muscle tissue (Rehberg et al. 2011).

SHG signal is produced in structures that exhibit non-inversion symmetry. Since SHG is produced in structures that exhibit this symmetry naturally, label-free imaging is possible (Sriram et al. 2019). SHG signal is produced in these structures when two photons of the same frequency interact with a material at a virtual state and combine to release one photon with twice the frequency, or one-half the wavelength (Figure 3) (Bueno et al. 2016). Since there is no absorption of a photon, there is in turn, no Stokes shift. Without a Stokes shift, no rotational and vibrational energy of the molecules is released as heat, and therefore photodamage and phototoxicity to the sample is significantly reduced (Pantazis et al. 2010). With the small focal volumes used in SHG microscopy, information regarding the semi-crystalline material being imaged such as its organization and ultrastructural properties can be determined (Cisek et al. 2017).

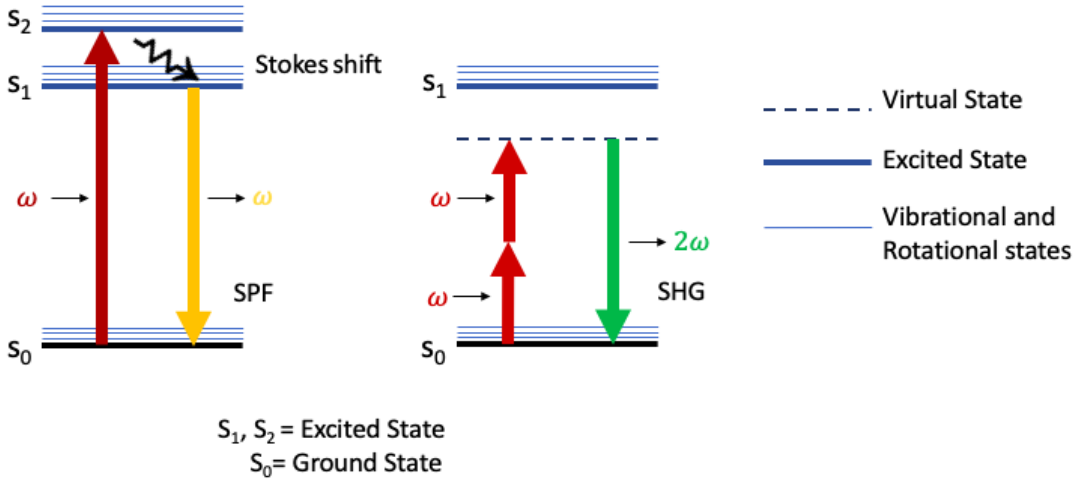

Figure 3: Energy state diagrams of single-photon excitation fluorescence (SPF) on the left and second harmonic generation (SHG) on the right. In SPF, a photon is absorbed, and therefore heat is released due to vibrational and rotational movements that occur during the Stokes shift. In SHG, two photons are converted to one, and as a result, no Stokes shift occurs, and no energy is dissipated into the system as heat (Pantazis et al. 2010).

The strength of the SHG signal is measured by the second-order nonlinear optical susceptibility tensor, $\chi^{(2)}$ (Samim et al. 2014). The $\chi^{(2)}$ value is a material property, and a non-zero value is dependent on the asymmetry of the molecules or the microcrystalline structure of the material (Ray 2010). In order to maximize the $\chi^{(2)}$ value, a few strategies can be used, such as optimizing the symmetry of the molecules or aligning them in such a way that an overall non-centrosymmetric macrostructure is achieved (Bueno et al. 2016). Calcite, the primary material found in otoconia is a centrosymmetric crystal and therefore based on previous theory, otoconia would not be expected to give SHG signal (Baconnier et al. 2002).

1.8 Study Objectives

The first objective of this study is to determine the origin of the SHG signal found in otoconia. By using polarization-sensitive SHG microscopy, the internal crystalline

properties of otoconia will be determined. SHG microscopy will allow for entire 3D imaging of the otoconia, and therefore using the organizational and structural information found by analyzing the polarization-sensitive images, the origin of the SHG signal will be determined (Tokarz et al. 2015). It is predicted that the SHG signal produced by otoconia is caused by the proteins embedded within the otoconia, which would indicate they are organized in a non-centrosymmetric fashion. Alternatively, the calcite could be giving SHG due to a quadrupole SHG effect, which does not have the symmetry restriction. A quadrupole occurs when molecules within the structure have two dipoles rather than just one, with alternating polarity. This allows SHG signal to be given off despite the symmetry of the structure (Stevenson and Maurice 2011). This effect is typically insignificant compared to standard dipole SHG so it would be surprising if this were the case (Bauer and Hingerl 2017). By determining the origin of the SHG signal in otoconia, information regarding the internal crystalline structure and how it interacts with the organic matrix will be deduced.

The second objective of this study is to determine how the structure of otoconia is altered when subjected to degrading chemical agents. Otoconia will be subjected to degrading agents such as ethylenediaminetetraacetic acid (EDTA), which is known for its ability to degrade calcium carbonate. Polarization-sensitive SHG microscopy will be used to determine how the ultrastructural properties of otoconia change at varying levels of degradation which can contribute to the development of an automated system for distinguishing between normal and altered otoconia. In future studies, this information could lead to improved treatments and drug delivery advancements for ototoxicity.

2. MATERIALS AND METHODS

2.1 Methods Summary

In order to complete the first study objective of determining the origin of SHG signal from otoconia, SHG microscopy images were taken of both otoconia and calcite crystals. By analyzing polarization-resolved images of these structures and comparing their SHG intensity levels, the origin of SHG signal was deduced.

The second study objective of this experiment was to determine how otoconia composition and structure is altered with degradation. This study objective was completed by exposing otoconia and calcite crystals to ethylenediaminetetraacetic acid (EDTA) which is a chemical known to degrade calcite. The otoconia and calcite crystals were imaged during degradation, and differences in SHG intensity levels of images were analyzed.

2.2 Temporal Bone Isolation

Mus musculus, or the common house mouse, was chosen as the model species to extract otoconia. The strain of mice used was Thy1-YFP B6TgCg 16Jrs/J, and all mice used were female. The mice were originally obtained from The Jackson Laboratory and bred at the Brain Repair Centre of Dalhousie University. The strain of origin of the mice was C57BL/6J, which is a very commonly used strain of laboratory mice due to their ability to breed quickly and their robustness (The Jackson Laboratory 2009) (Maga 2016). To avoid age-related structural irregularities, mice between 40-60 days old were used (Jang et al. 2006). The mice were housed two per cage with food and water as needed, prior to being

sacrificed for the purpose of this pilot study (Protocol #I20-04). All procedures described were approved by the Dalhousie University Animal Care and Use Committee.

To begin isolation of otoconia, a mouse was given a lethal intraperitoneal injection of 340 mg/mL Euthasol® pentobarbital (Merck Animal Health) with a dose of 250 mg per kg. It was then placed back into its enclosure for approximately two minutes until fully unresponsive. Next, the mouse was pinned down and transcardially perfused in order to remove all blood from the body. It was essential to perfuse the mouse as quickly as possible to ensure the heart continued beating for the procedure to be effective.

To begin perfusion, an incision, approximately 5 centimeters long, was made through the integument and abdominal wall directly below the rib cage using surgical scissors. The liver was then separated from the diaphragm. Using the same scissors, an incision was made along the entire length of the diaphragm in order to expose the pleural cavity. A longitudinal cut was made from the bottom of the rib cage up to the collarbone. The sternum was then carefully lifted and cut out of the way so that the heart was adequately exposed. Any tissue surrounding the heart was trimmed away to allow better access for perfusion. A 26-gauge butterfly perfusion needle was then inserted into the left ventricle, and a small incision (~2 mm) was made into the right atrium. Next, 300 mL of isotonic saline prepared in house was carefully pushed into the left ventricle until all blood exited the right atrium. It was essential not to push the solution through the body too forcefully to prevent bursting any blood vessels.

2.3 Otoconia Isolation

Following perfusion, the mouse's head was removed using large surgical scissors. In addition, the external auditory canals were cut off, and the skin was pulled forward towards the nose. The following procedure for otoconia isolation was modified from that used by Ou, Lin, and Rubel (2013). After decapitation, the skull was bisected along the sagittal suture using a #11 scalpel. The brain and any excess muscle were removed from both sides of the skull. The temporal bones were then isolated by trimming away any surrounding areas of the skull. Isolated temporal bones were stored in 0.1 M sodium cacodylate buffer (pH 7.4) (Sigma Aldrich) until completion of otoconia isolation took place. The 0.1 M sodium cacodylate buffer (pH 7.4) was prepared by measuring 2.14 g of sodium cacodylate powder (Sigma Aldrich) and then adding ~80 mL of deionized water. HCl was then added until a pH of 7.4 was achieved by monitoring with a pH meter and the final volume was brought to 100 mL using deionized water. To begin isolation, the temporal bone was placed onto a petri dish under a VanGuard® dissecting microscope. The anterior semicircular canal was located in order to be used as a landmark to find the utricle. As shown in Figure 4, perpendicular to the anterior semicircular canal lies the petrous ridge. Just above the petrous ridge, there is a small area of translucent bone that was carefully removed using a fine bone pick. Just below this bone lies the utricle, which was removed using #5 forceps.

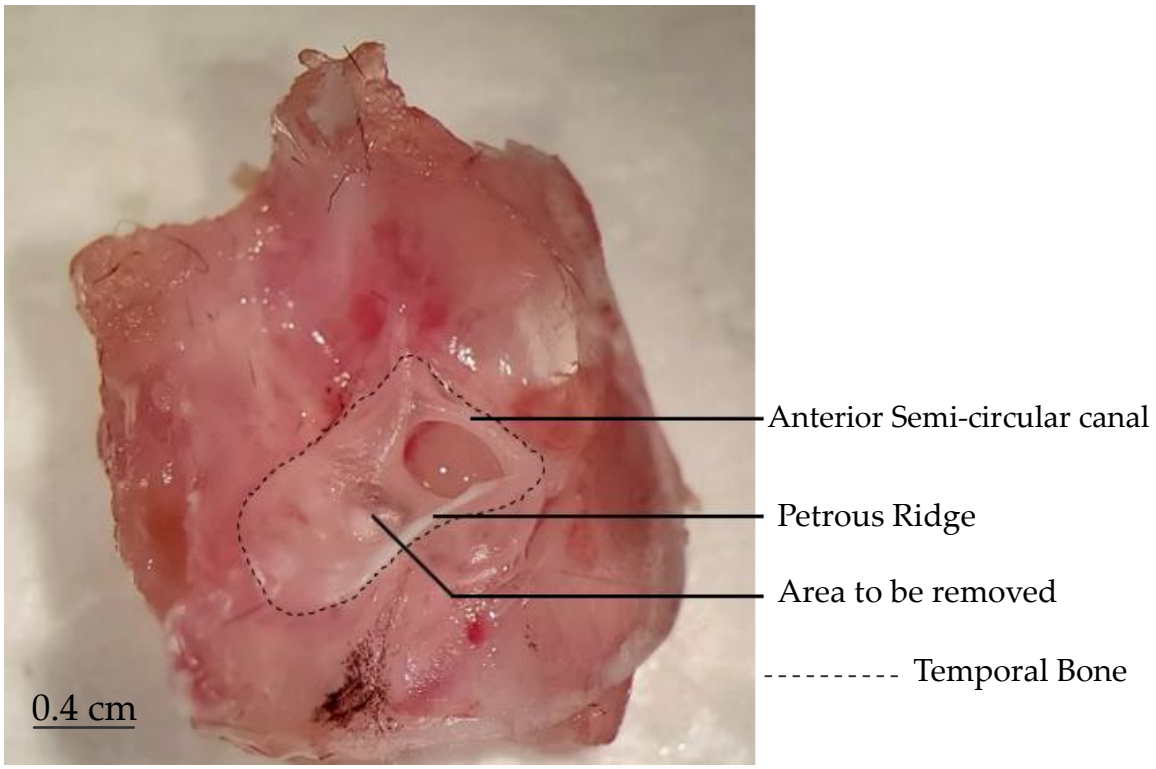

Figure 4: The temporal bone of a common house mouse (*mus musculus*), before removal of the utricle. Mice specimens were obtained and dissected at the Brain Repair Centre of Dalhousie University. The area to be removed as indicated in the figure was carefully lifted using forceps and the utricle containing otoconia was then removed for imaging.

2.4 Second Harmonic Generation Microscopy

In order to acquire images using SHG microscopy, a custom built non-linear optical microscope was used. The laser source used was a 1030 nanometer (nm) wavelength, ultrafast laser (FemtoLux 3, Ekspla) with a 5-megahertz (MHz) repetition rate, and 240 femtosecond (fs) pulse duration. The laser was coupled to a custom non-linear optical microscope. Galvanometric scanning mirrors were used to raster scan the laser beam across the sample. For focusing, an air immersion objective lens with a 0.8 numerical aperture (NA) (Plan-Apochromat 20×, Carl Zeiss AG) was used. SHG signals were filtered using interference and absorptive filters (65-129 and 48-637, Edmund Optics Inc.) and were

collected using a custom-built 0.8 NA objective lens. The signals were detected using a photomultiplier tube in photon counting mode (H1062-210 Hamamatsu). In order to perform polarization measurements, the microscope was modified by adding a linear polarizer, a quarter-wave plate, and a liquid crystal polarization retarder before the excitation objective lens (Figure 5), which functioned to form circularly polarized light or rotate the orientation of the linearly polarized incident beam. The beam was subsequently focused to a small spot via a microscope objective lens. SHG images were analyzed by first defining an XYZ coordinate system with respect to Y, which is the primary propagation of the laser beam and XZ, which is the image plane (Figure 5).

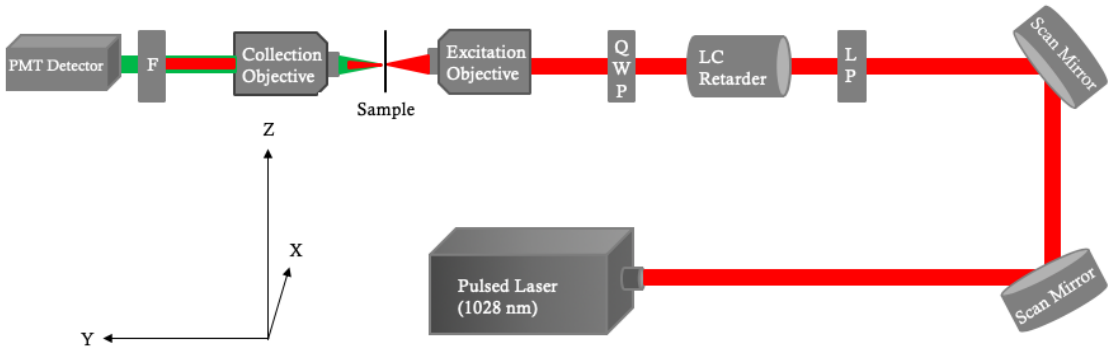

Figure 5: A schematic of the home-built non-linear optical microscope set-up used to acquire SHG images. The following abbreviations are used: LP- linear polarizer, QWP- quarter-wave plate, LC- liquid crystal, F- filter and, PMT- photomultiplier tube. Schematic of the XYZ coordinate system used.

2.5 Calcite

Two small pieces (approximately 2 cm × 2 cm) of impure and pure calcite were acquired from Prof. Hanley of the Geology department at Saint Mary's University. Using a porcelain mortar and pestle, the crystals were separately ground down until a fine powder resulted. Approximately 0.2 g of the calcite powder was placed into an Eppendorf tube

containing 1 mL of 0.1 M sodium cacodylate buffer (pH 7.4) to expose the calcite crystals to the same environment that the otoconia samples were placed in. The solution in the Eppendorf tube was mixed by closing the lid and shaking the solution. Quickly, while the crystal powder was still suspended in the buffer solution, 50 μL was removed using a micropipette and placed onto a 75 × 25 mm microscope slide (Fisher Scientific). The solution was then covered by a 24 × 40 mm coverslip (Fisher Scientific) and sealed with clear Sally Hansen® nail polish for SHG imaging. This procedure was performed for both the pure and impure calcite samples.

In order to simulate a similar environment to the gel-like region of the cupula that otoconia reside in, calcite particles were also imaged while suspended in polyacrylamide gel. A mixture of polyacrylamide mix was assembled by combining 1.5 g acrylamide powder (Sigma Aldrich), 0.04 g bisacrylamide powder (Sigma Aldrich), and 5 mL of deionized water. APS mix was next assembled by combining 0.1 g of ammonium persulfate (APS) (Sigma Aldrich) and 0.9 mL of deionized water. Next, 200 μL of the 0.1 M sodium cacodylate buffer pH 7.4 (Sigma Aldrich) with calcite powder solution, 40 μL of polyacrylamide mix, 10 μL of APS mix, and 1 μL of tetramethylethylenediamine (TEMED) (VWR) was placed into an Eppendorf tube using a micropipette. After the addition of TEMED, the Eppendorf tube was immediately closed and shaken to mix. A micropipette was then used to remove 20 μL of the solution and was placed onto a glass slide for SHG imaging before complete gelling occurred. The solution was covered with a coverslip and sealed using Sally Hansen® clear nail polish.

Due to the small particle size of the pure calcite powder larger pure calcite crystals were grown in house in order to ensure SHG signal could be detected. The crystals were

grown by supersaturating the pure calcite powder using deionized water and ethanol separately to determine the most effective solvent. The most effective solvent was determined to be deionized water. Once supersaturated, each solution was placed onto a separate petri dish with a paperclip to be used as a nucleation site for crystal formation. The petri dishes were then left for 48 hours until crystallization was complete. The powder was then placed onto a glass slide and then covered with a coverslip and sealed using Sally Hansen® clear nail polish to be imaged.

2.6 Otoconia and Calcite Degradation Experiments

The effects of chemical degradation on otoconia were studied by exposing them to EDTA (Sigma Aldrich). To begin, otoconia were placed onto a 75 × 25 mm microscope slide (Fisher Scientific) immersed in 0.1 M sodium cacodylate buffer (pH 7.4). They were then covered with a 24 × 40 mm coverslip (Fisher Scientific), which was then sealed onto the slide for imaging using clear Sally Hansen® nail polish. SHG images were then taken to act as a control before degradation of the otoconia took place. Once sufficient images of three control otoconia were acquired, and their positions were recorded, the slide was removed.

In order to degrade otoconia, a 5 mL BD® syringe with a 25 G needle was carefully inserted approximately 0.5 cm forwards underneath the coverslip just above the sample on the slide, and the plunger was slowly pushed in order to flush the otoconia with 0.5 M EDTA. Immediately after exposing the otoconia to EDTA, a timer was started to keep track of how much time had elapsed. The slide was then quickly placed back onto the microscope stage, and the same three control otoconia were located using a home-built program on

LabVIEW to move the stage between their previously recorded positions. Data collection took place over approximately 90 minutes. Images were taken approximately every ten minutes, alternating between the three located otoconia in order to observe EDTA degradation over time.

A similar procedure was followed in order to observe EDTA degradation of calcite with time. Calcite mineral was crushed using a marble mortar and pestle and placed onto a 75 × 25 mm microscope slide (Fisher Scientific). The calcite was then covered with a 24 × 40 mm coverslip (Fisher Scientific), which was then sealed onto the slide for imaging using clear Sally Hansen® nail polish. Control images of calcite were then taken prior to EDTA exposure. Once adequate control images were taken the slide was removed. A 5 mL BD® syringe with a 25 G needle was next carefully inserted approximately 0.5 cm forwards underneath the coverslip just above the sample on the slide, and the plunger was slowly pushed in order to flush the calcite with 0.5 M EDTA. A timer was immediately started, and the slide was placed onto the microscope stage for SHG imaging. A suitable region of calcite was chosen to image over a period of ~90 minutes in order to observe degradation of calcite with time.

2.7 Analysis Methods

SHG intensity of the otoconia and calcite was deduced by analyzing the SHG images on ImageJ (NIH). Using ImageJ, the maximum SHG intensity of background noise in the image was determined by increasing the brightness until the maximum noise level could be determined. Using the thresholding function the lower threshold was set to the maximum background noise level. Mean SHG intensity of otoconia and calcite along with

their standard errors was then calculated using the remaining image after thresholding using the Analyze function in Image J. SHG intensity levels of otoconia were compared at both linear and circular polarizations. Trends were also visualized by plotting the calculated mean otoconia and calcite intensity over time after EDTA degradation.

3. RESULTS

3.1 Calcite Mineral SHG Imaging

Calcite mineral was prepared and imaged following the procedures outlined in section 2.7 in order to determine if calcite crystal gives SHG signal. Due to the fact that calcite makes up >90 wt. -% of otoconia, it is likely that if calcite gives SHG signal, that it would be the origin of SHG signal. The calcite crystals were first imaged in 0.1 M sodium cacodylate buffer solution (pH 7.4). All images for this first experiment were obtained using linearly polarized laser light. It was observed that the entire calcite mineral gave SHG however, it was noted that there was intense SHG signal in localized regions rather than dispersed uniformly throughout the calcite crystal. This is surprising as it would be expected that the entire crystal would give similar SHG signal. For example, the bright region circled in red in Figure 6 had a mean SHG intensity of 333 ± 11 photon counts whereas the yellow circle (dashed) in the same image had an mean SHG intensity of 15 ± 0.4 photon counts making it approximately 22× lower in intensity.

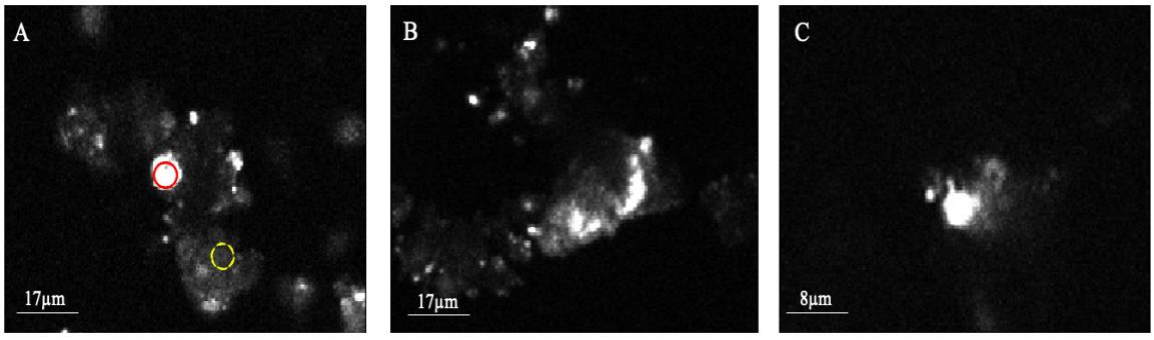

Figure 6: Second harmonic generation microscopy images of calcite mineral in 0.1 M sodium cacodylate buffer (pH 7.4). The red circle in image A is indicating a region of high SHG intensity, compared to the yellow circle (dashed) that is showing a comparitively low region of SHG signal.

As shown in Table 1, when all of the SHG intensities are standardized to a 7.2 mW power level, image A had a mean SHG intensity approximately 16× greater than images B and C. It was noted that the high intensity observed in Image A was an anomally when compared to the intensity of calcite in other images taken in both calcite experiments.

Table 1: The standardized SHG intensities of calcite mineral imaged in 0.1M sodium cacodylate buffer. Mean SHG intensity was calculated using ImageJ by thresholding the background noise level and obtaining the mean intensity of calcite mineral.

Image	Power (mW)	Mean SHG Intensity (photon counts)	Standardized SHG Intensity (7.2 mW)	Standard Error (photon counts)
A	1.6	84	650	20
B	7.2	41	41	5
C	7.2	37	37	7

In a second experiment, the same calcite mineral was imaged using SHG microscopy; however, the calcite was imaged in acrylamide gel in addition to 0.1 M sodium cacodylate buffer (pH 7.4) in order to simlulate the gel-like environment within the inner ear. All calcite mineral images were taken using a linear polarization. Morphologically the calcite images for this experiment were very similar to the first experiment and SHG intensity was again localized to very intense regions rather than dispersed throughout the crystal. For example, in image A the bright region circled in red had an SHG intensity of 320 ± 10 photon counts whereas the darker region circled in yellow (dashed line) had an SHG intensity of 27 ± 1 photon counts making it approximately 12 × lower (Figure 7).

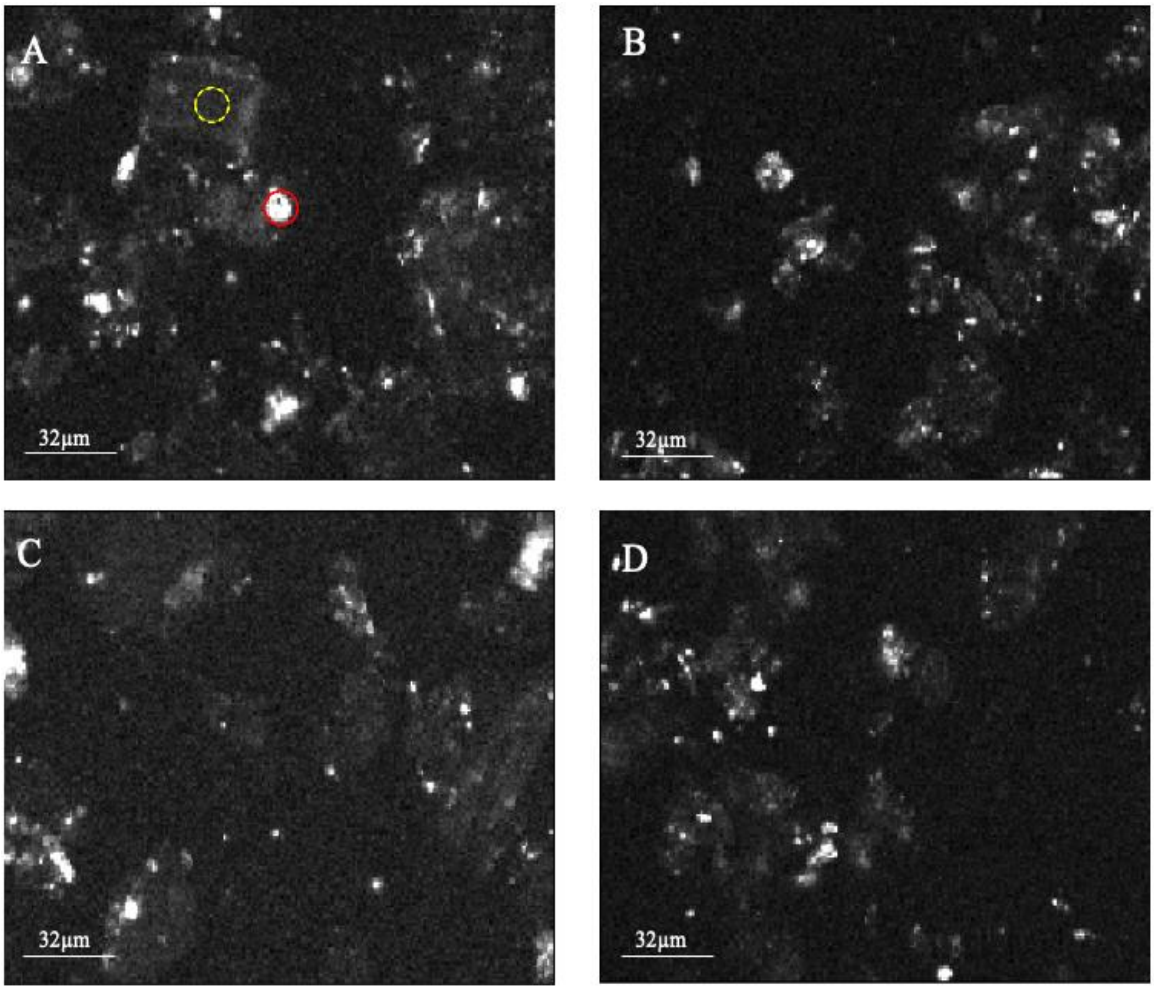

Figure 7: SHG microscopy images of calcite mineral in acrylamide gel and 0.1M sodium cacodylate buffer (pH 7.4). The red circle in image A is indicating a region of high SHG intensity, compared to the yellow circle (dashed) that is showing a comparitively low region of SHG signal.

The mean SHG intensities of these images shown in Table 2, were relatively similar with the average of the mean SHG intensities being 52 ± 5 photon counts. Due to the fact that all images were taken using the same power level, standardization of the signal was not necessary.

Table 2: Mean SHG Intensities for calcite mineral imaged with acrylamide gel and 0.1M sodium cacodylate buffer (pH 7.4). Mean SHG intensity was calculated using ImageJ by thresholding the background noise level and obtaining the mean intensity of calcite mineral.

Image	Power (mW)	Mean SHG Intensity (photon counts)	Standard Error (photon counts)
A	7.2	47	5
B	7.2	53	3
C	7.2	48	3
D	7.2	58	5

3.2 Purified Calcite SHG Imaging

Due to the non-uniformity of signal observed in calcite mineral, a sample of purified calcite crystal powder was imaged in 0.1 M sodium cacodylate buffer (pH 7.4) following the procedures outlined in section 2.7. The imaging was performed using up to 26 mW power; however, no SHG signal was detected from the purified calcite sample (Figure 8). Image B was taken in the same position and zoom setting as image A; however, it was imaged using third harmonic generation (THG) microscopy to verify there were crystals within the image region. The crystals were visible using THG microscopy verifying that the lack of SHG signal in image A was not due to instrumental error.

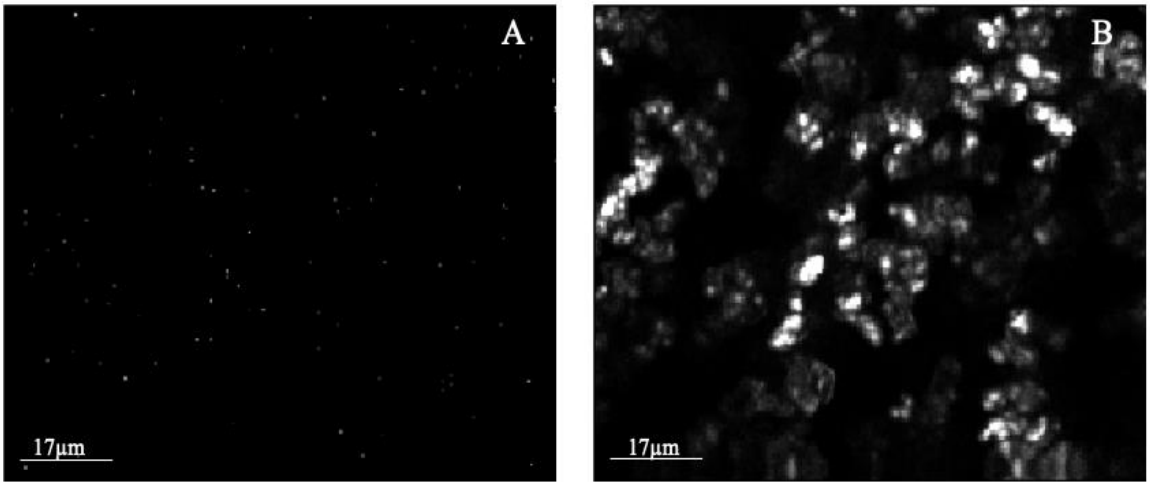

***Figure 8*:** Pure calcite crystals imaged using (A) second harmonic generation microscopy and (B) third harmonic generation microscopy. Purified calcite powder was immersed in 0.1M sodium cacodylate buffer (pH 7.4) for imaging.

Larger pure calcite crystals were also grown in house order to make sure the particle size of the pure calcite powder was not too small, following the procedures outlined in section 2.7. Low amounts of SHG signal were detected from the larger crystals as shown in Figure 9. Despite the SHG signal that was detected it is still ~41× lower than the signal observed with otoconia, so it is unlikely that calcite is responsible for the origin of SHG signal in otoconia.

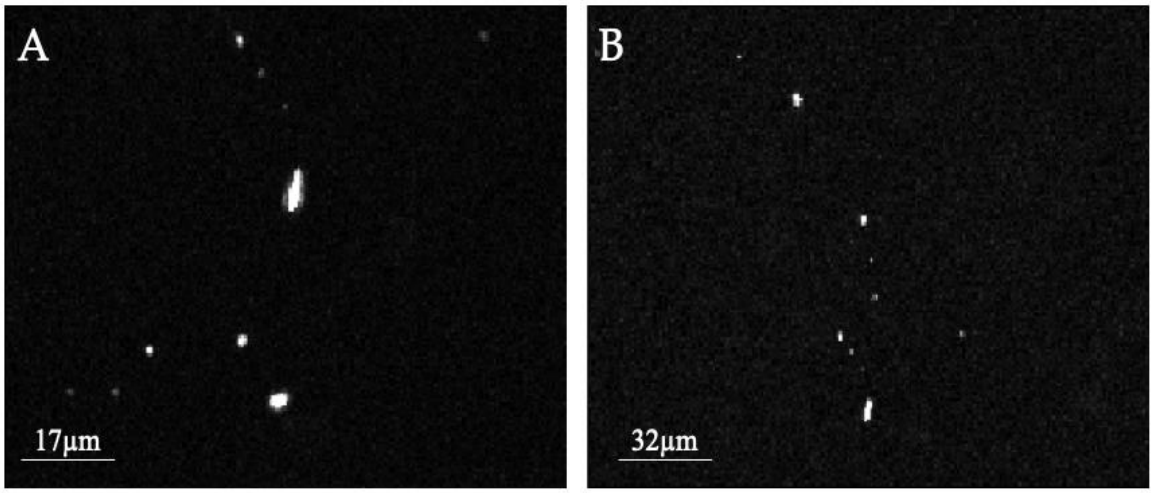

Figure 9: SHG microscopy images of pure calcite crystals grown to a larger particle size. The crystals in images A and B were grown in deionized water for 48 hours and immersed into 0.1M sodium cacodylate buffer (pH 7.4) for imaging.

3.3 Calcite EDTA Degradation Over Time

A sample of calcite mineral was imaged over a period of 90 minutes while exposed to 0.5 M EDTA, which is a chemical known to have the ability to degrade calcium carbonate (Figure 10). Calcite mineral was exposed to EDTA in order to determine how the degradation of calcite compares to that of otoconia, and how the SHG signal is affected in each case. The procedure outlined in section 2.6 was followed to prepare and image the sample. The calcite mineral was imaged using circularly polarized light. Images were taken using a zoom setting of 194 µm × 160 µm.

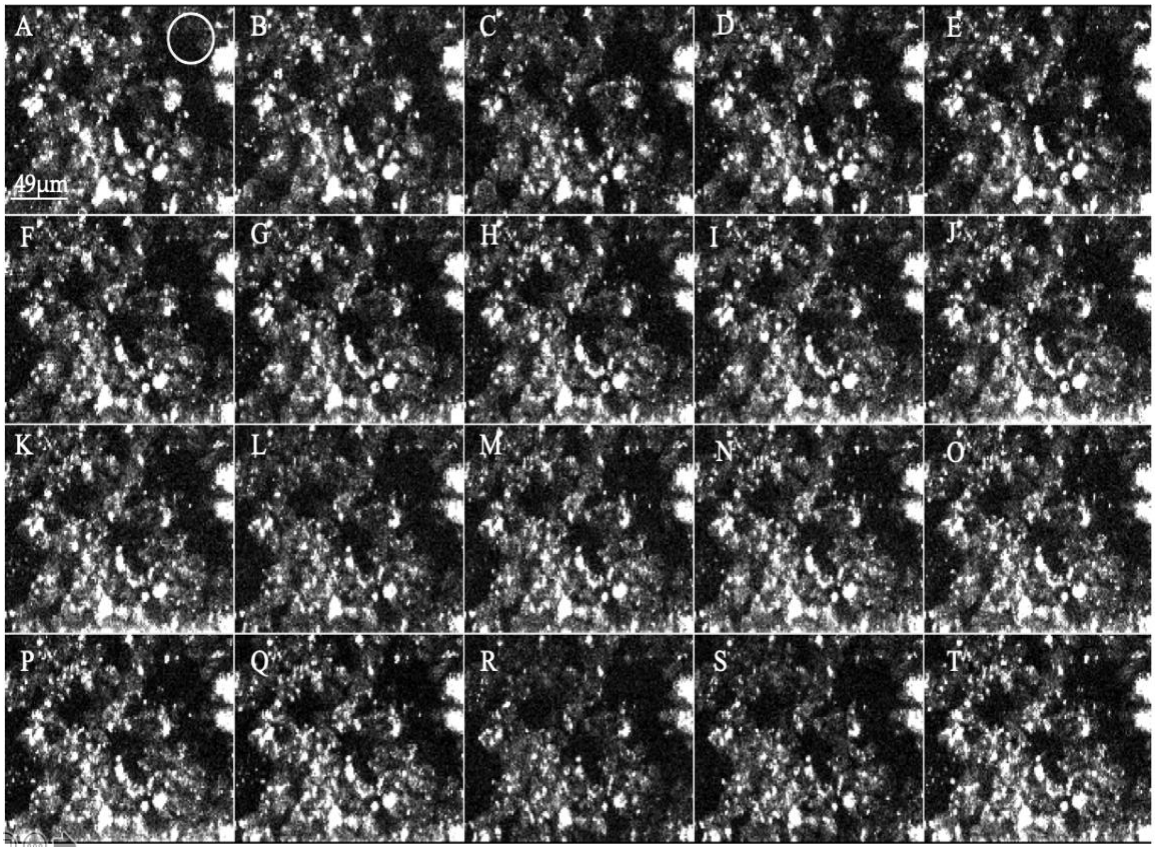

Figure 10: Calcite mineral in 0.5M EDTA imaged using SHG microscopy over a period of 90 minutes. A-T represent subsequent images taken approximately every 4 minutes. Scale Bars from B-T are equivalent to that shown in A. All images were taken using circularly polarized light as indicated by the circle in the top right corner of image A.

As shown in Figure 11 there was no overall increase or decrease observed in mean SHG intensity over the 90 minutes of degradation. This figure was acquired from ImageJ and is showing the calculated mean SHG intensity for each of the 20 images taken over the 90-minute period. Although slight fluctuations in signal were observed, they were very minor (the largest fluctuation was ~2.3 photon counts from the intensity of the first image). These fluctuations are likely due to the manual optimization of the Z plane which was performed for each image. Overall, the mean SHG intensity from the first image to the last shifted ~1 photon count and therefore it was determined that degradation of calcite mineral using EDTA does not cause a large increase or decrease in SHG signal.

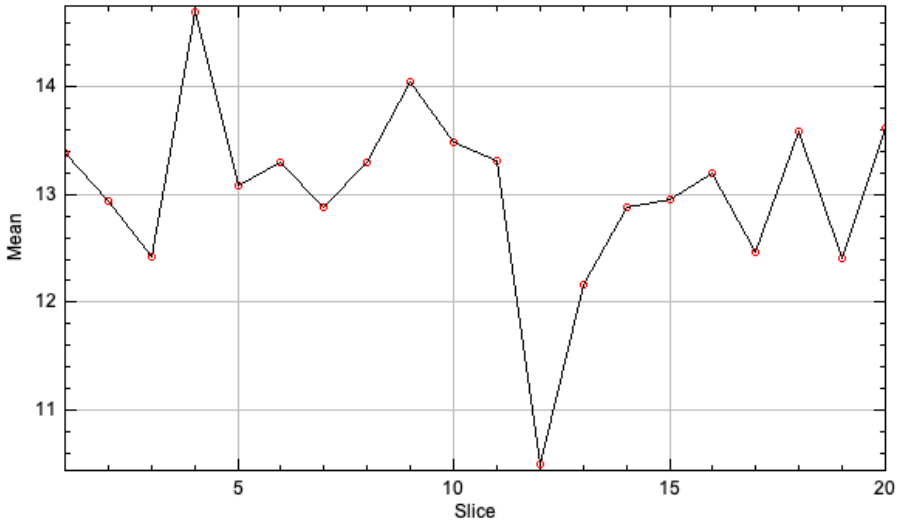

Figure 11: The mean SHG intensity of subsequent images of calcite mineral in 0.5M EDTA. Each slice of the graph represents approximately 4-minute intervals for a total of approximately 90 minutes . The mean SHG intensities were calculated using ImageJ.

3.4 Otoconia SHG Imaging

Otoconia were isolated from the utricle of mice and imaged using SHG microscopy using the procedures outlined in section 2.3. When linearly polarized light was used on

otoconia it was observed that two lobes become visible with a darker region between them as seen in Figure 12. Using linearly polarized light otoconia were observed to give varying mean SHG signals with a range of 99 ± 5 photon counts to 1030 ± 30 photon counts at a standardized power level of 3.7 mW. Images A and B in Figure 12 are showing the same otoconia imaged using different polarization angles. A completely different portion of the otoconia becomes visible when using a different linear polarization. Images C and D are also the same otoconia imaged using different linear polarizations. In some otoconia it appears that there are fracture lines in certain regions within them. An example of these fracture lines can be seen in the red circled region of image A of Figure 12.

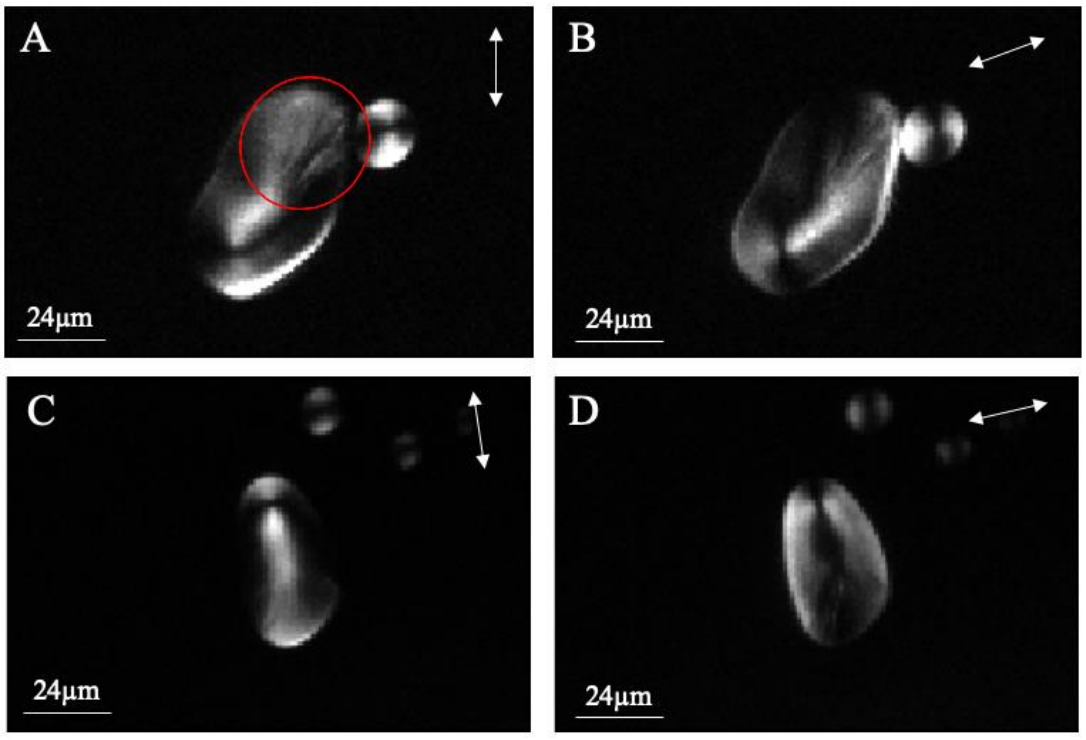

Figure 12: Otoconia imaged using SHG microscopy at two different linear polarizations indicated in the top right-hand corner of the images. Images A and B are showing the same otoconia but are different from the ones pictured in images C and D which are also the same. The red region circled in image A is showing what appears to be fracture lines within the otoconia.

Otoconia were observed to be polarization-dependent when using linearly polarized light. This polarization dependence means that as the angle of the laser beam linear polarization is rotated (i.e. the polarization is changed), a different region of the otoconia becomes visible within the two lobes. The images in Figure 13 are showing the otoconium at eight different polarization angles.

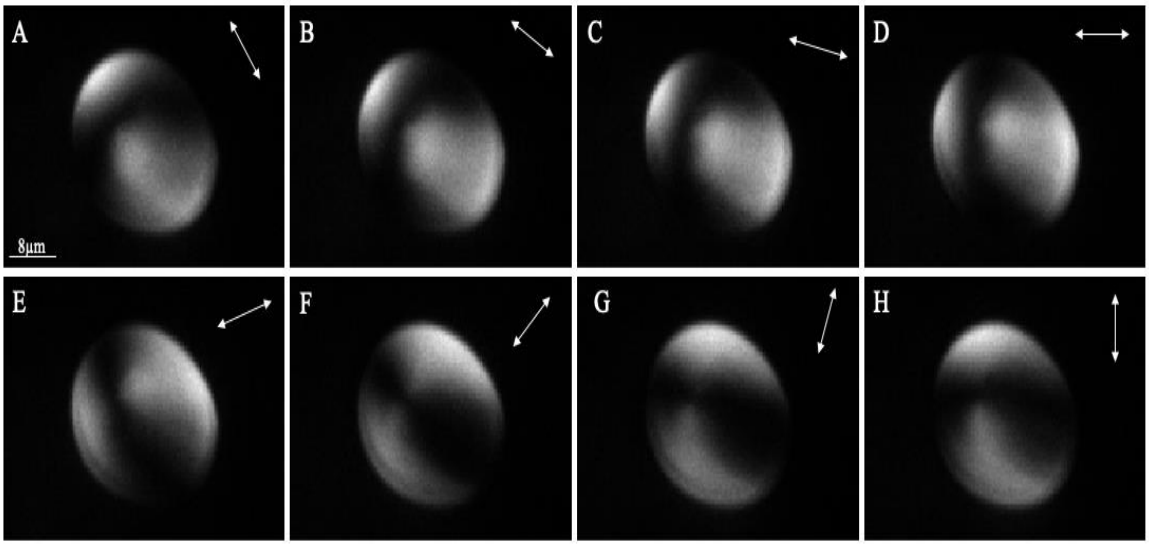

Figure 13: A single otoconium imaged using SHG microscopy at eight polarization angles (A-H). The linear polarizations are indicated in the top right-hand corner of the images. The scale bars for images B-H are equivalent to that shown in image A.

When circularly polarized light is used on otoconia, the lobes disappear and the entire otoconia gives SHG signal allowing them to be seen as a whole. Outer rings along the outer edges of some otoconia were visible when using circularly polarized light was used as shown in the otoconia in image A of Figure 14. It was also noted that when otoconia were imaged with circularly polarized light there was a small dark circular region near the centre of each otoconia where no SHG signal was given (Figure 14).

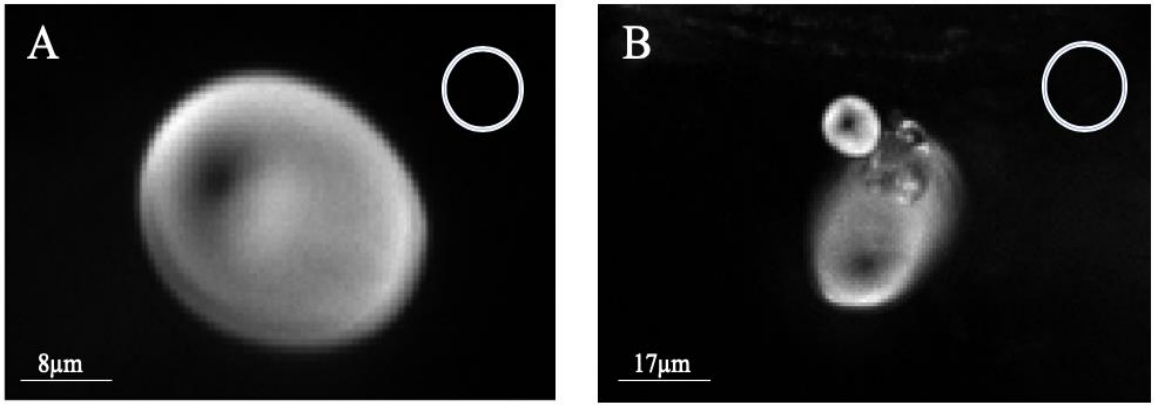

Figure 14: Otoconia imaged with SHG microscopy using circularly polarized light. The circular polarization is indicated in the top-right corner. The entire otoconium is visible when using circularly polarized light.

3.5 Otoconia EDTA Degradation Over Time

Three otoconia were imaged while being exposed to 0.5 M EDTA using the procedures outlined in section 2.6 in order to determine how SHG signal is altered with degradation. The SHG signal of each of the three otoconia was measured over a period of ~80 minutes. All intensities for all three otoconia were standardized to a power level of 3.7 mW to facilitate comparisons and all were imaged using the same linear polarization. As shown in Figure 15 in the beginning of the experiment otoconia #1 was determined to have a mean intensity of 147 ± 14 photon counts which then increased with time until after 53 minutes had passed and the SHG signal was determined to be 203 ± 21 photon counts. After 53 minutes the signal began to plateau and did not increase or decrease in large increments for the rest of the experiment.

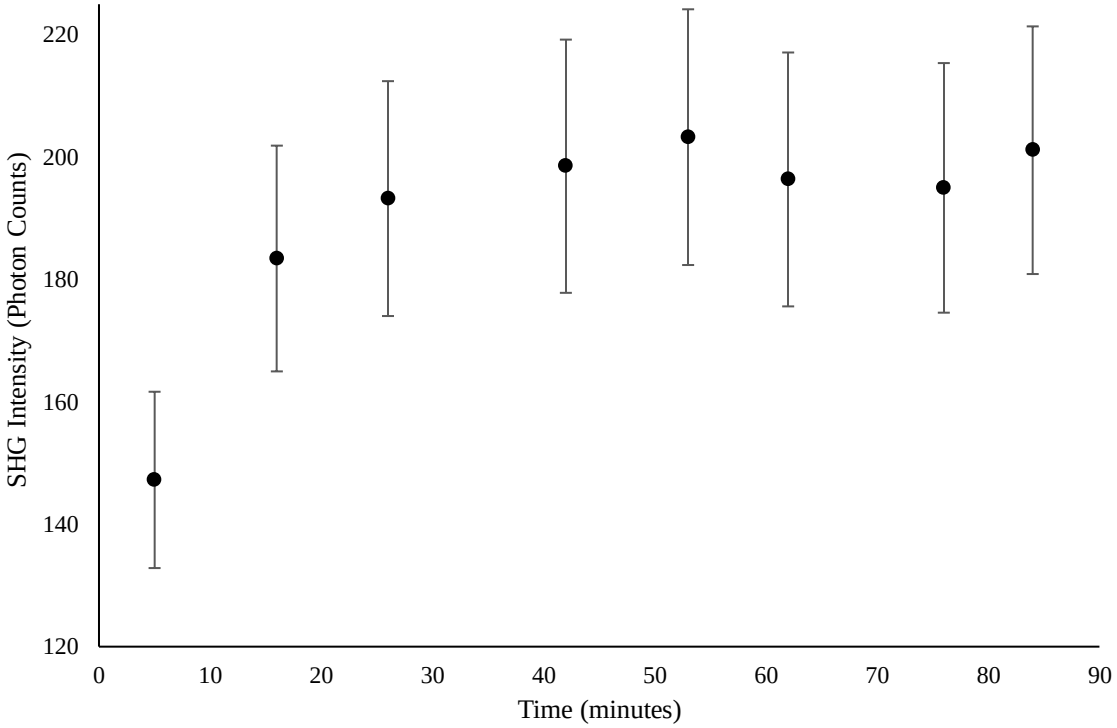

Figure 15: The SHG intensity of otoconium #1 imaged over a period of 84 minutes while being exposed to 0.5 M EDTA. The error bars represent +/- one standard error.

Figure 16 is showing otoconia #1 with image A being the first imaged taken after exposure to EDTA and image B showing the last. Image B has a visibly higher SHG intensity compared to image A. In particular one region that increased is circled in red on image A had a mean SHG intensity of 356 ± 1 photon counts whereas in image B the same region had a mean SHG intensity of 738 ± 6 photon counts.

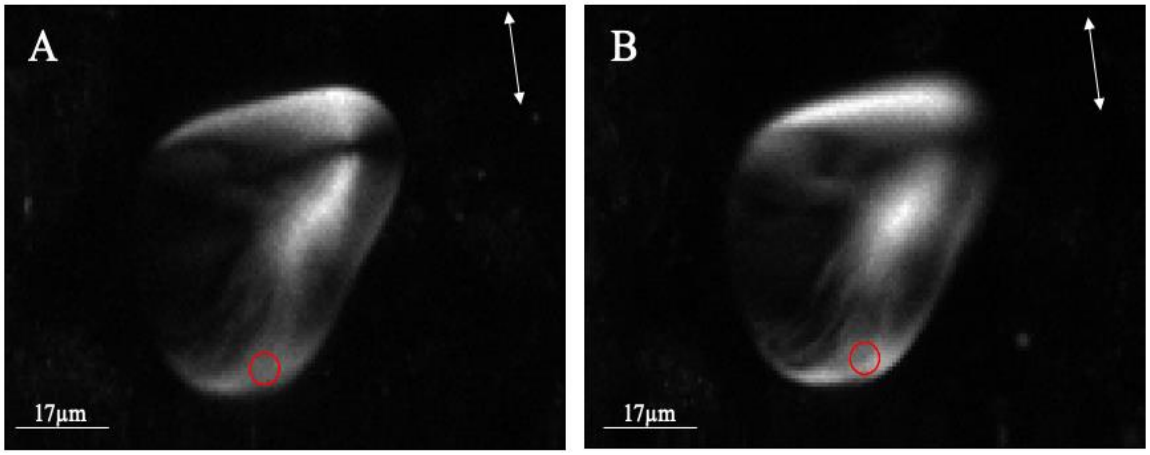

Figure 16: Otoconium #1 imaged after exposure to 0.5 M EDTA at the (A) beginning of the experiment (first image taken) and (B) end of the experiment (last image taken) after 84 minutes. The linear polarizations are indicated in the top right-hand corner of the images.

As depicted in Figure 17 a similar trend was observed for otoconia #2. At the beginning of the experiment otoconia #2 was determined to have a mean intensity of 650 ± 30 photon counts which then increased with time until after 29 minutes had passed where the SHG signal was determined to be 750 ± 30 photon counts. After 29 minutes the signal began to plateau and did not increase or decrease in large increments for the rest of the experiment.

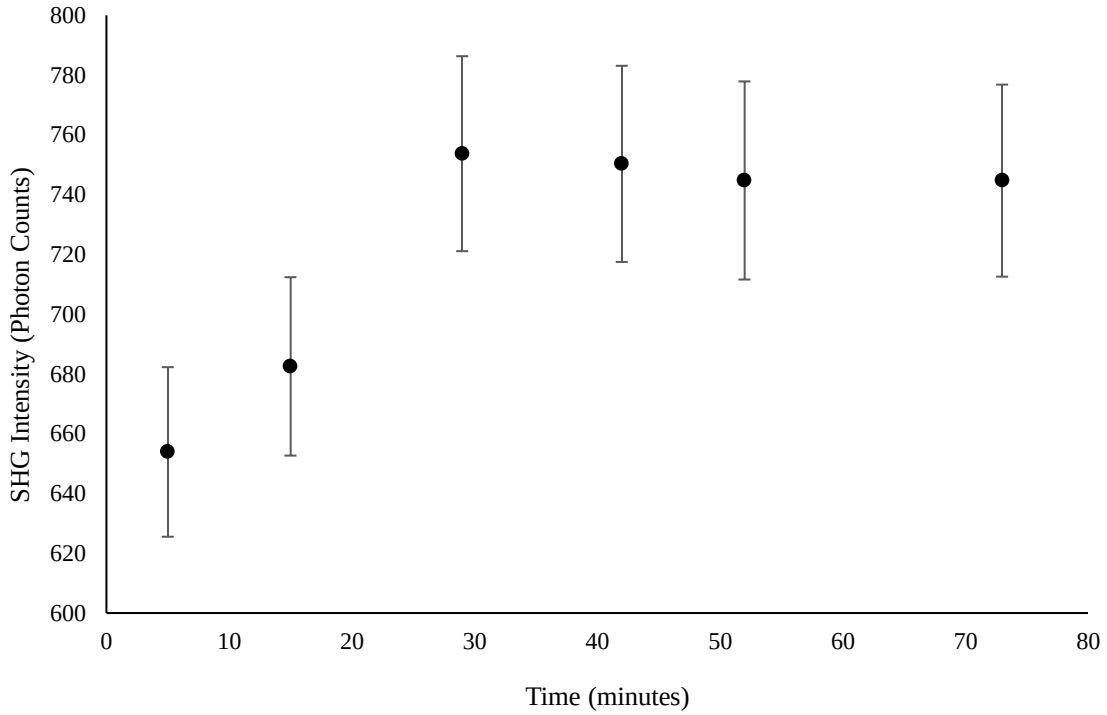

Figure 17: The SHG intensity of otoconium #2 imaged over a period of 73 minutes while being exposed to 0.5 M EDTA. The error bars represent +/- one standard error.

Figure 18 is showing otoconia #2 with image A being the first imaged taken after exposure to EDTA and image B showing the last. Again, image B has a visibly higher SHG intensity compared to image A. In particular one region that increased is circled in red on image A had a mean SHG intensity of 1030 ± 10 photon counts whereas in image B the same region had a mean SHG intensity of 1249 ± 8 photon counts.

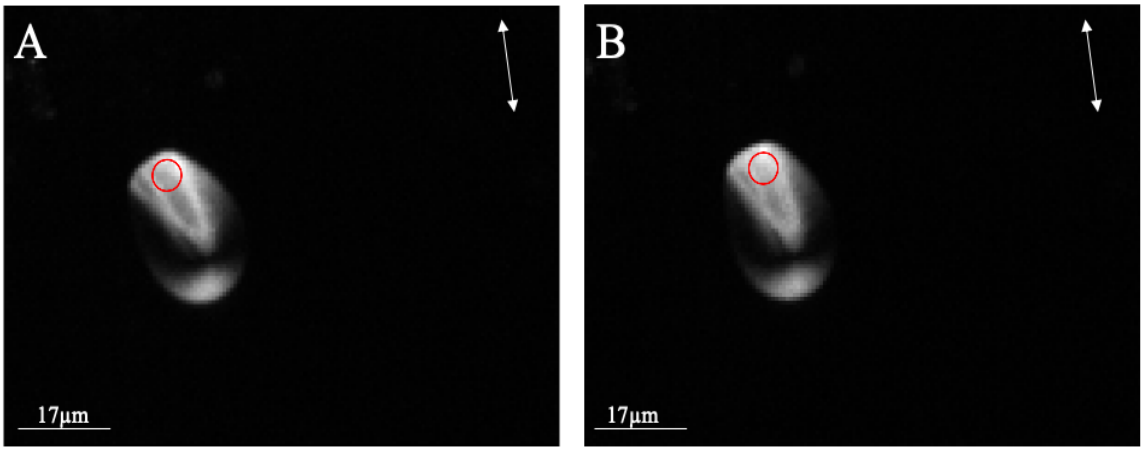

Figure 18: Otoconium #2 imaged after exposure to 0.5 M EDTA at the (A) beginning of the experiment (first image taken) and (B) end of the experiment (last image taken) after 73 minutes. The linear polarizations are indicated in the top right-hand corner of the images.

Figure 19 is showing the mean SHG intensity of otoconia #3 after exposure to 0.5 M EDTA for a period of 74 minutes. At the beginning of the experiment otoconia #3 was determined to have a mean intensity of 820 ± 30 photon counts which then increased with time until after 29 minutes had passed where the SHG signal was determined to be 1030 ± 30 photon counts. After 29 minutes the signal began to plateau and did not increase or decrease in large increments for the rest of the experiment.

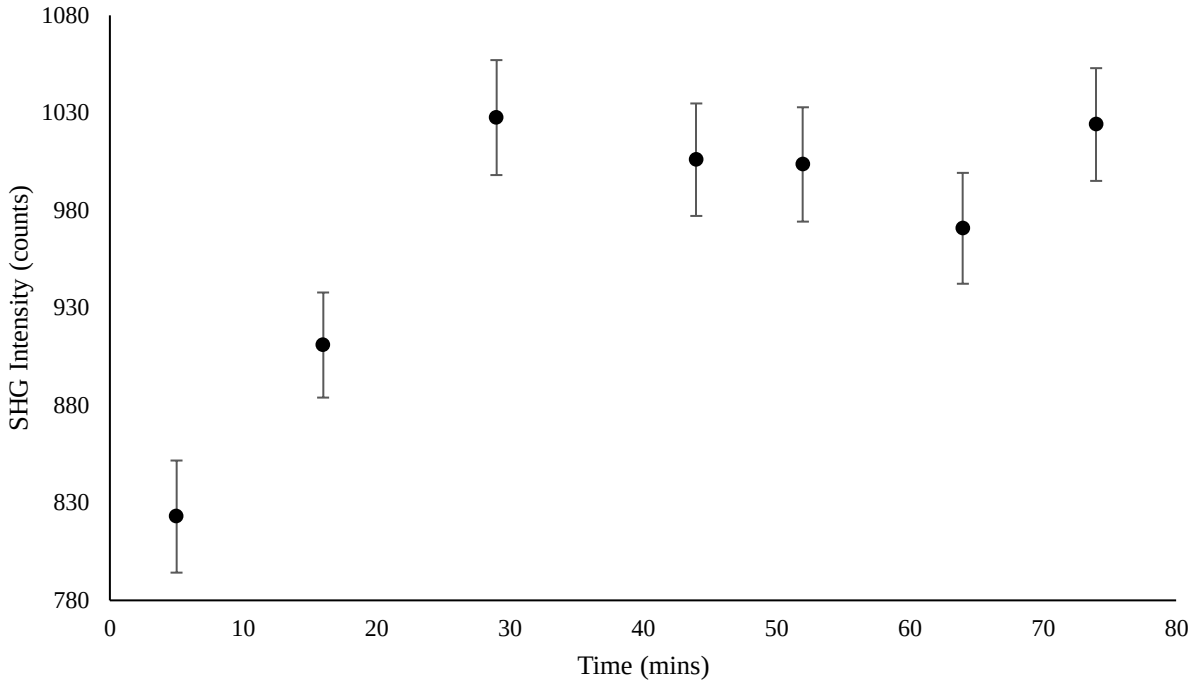

Figure 19: The SHG intensity of otoconium #3 imaged over a period of 74 minutes while being exposed to 0.5 M EDTA. The error bars represent +/- one standard error.

Figure 20 is showing otoconia #3 with image A being the first imaged taken after exposure to EDTA and image B showing the last. Similarly, an increase in SHG signal was observed between the two images. In particular one region that increased is circled in red on image A had a mean SHG intensity of 421 ± 3 photon counts whereas in image B the same region had a mean SHG intensity of 501 ± 4 photon counts.

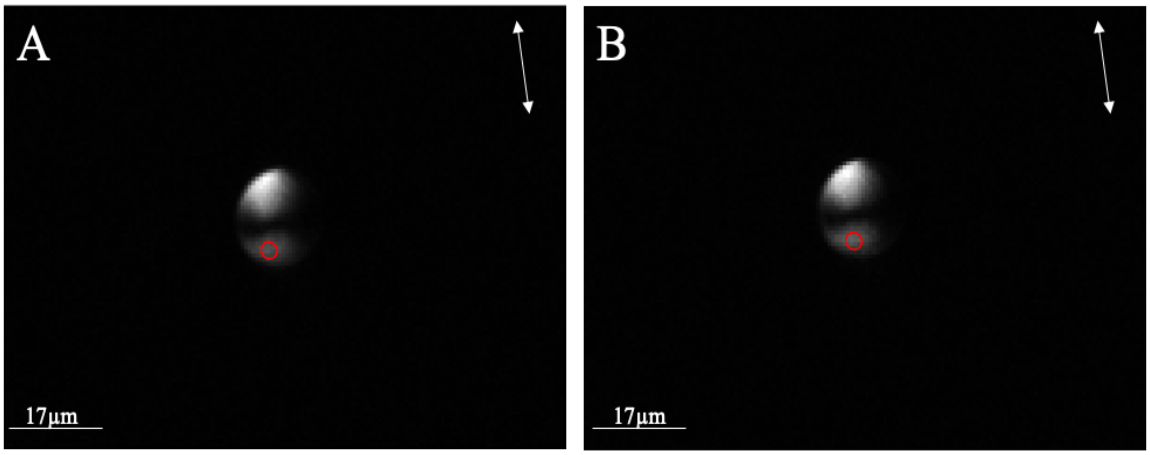

Figure 20: Otoconium #3 imaged after exposure to 0.5M EDTA at the (A) beginning of the experiment (first image taken) and (B) end of the experiment (last image taken) after 73 minutes. The linear polarizations are indicated in the top right-hand corner of the images.

4. DISCUSSION

4.1 Study Objective 1: Determine the Origin of SHG signal in Otoconia

In order to determine the origin of SHG signal in otoconia, calcite mineral was imaged using SHG microscopy. The calcite mineral was observed to give ~8× less SHG signal when compared to otoconia. At first, this seemed like it could likely be responsible for the SHG signal given in otoconia as calcite makes up ~95% of the otoconia. However, as shown in Figure 5, the majority of intense signal was localized in small regions rather than dispersed uniformly throughout the crystal, which was unusual.

For this reason, pure calcite powder was imaged, and no SHG signal was detected. This indicates that the regions of high intensity from the calcite mineral may have been caused by inclusions. When a mineral is formed underground, impurities known as inclusions are often incorporated into developing crystals (Roedder 1962). Typically, inclusions are other minerals or rocks, but can sometimes be trapped fluids or gasses as well (Harnisch et al. 2000). This is a potentially interesting area of future research as SHG microscopy could be used in the future to detect inclusions trapped inside crystals. This explains why intense SHG signal was localized to particular regions rather than dispersed uniformly throughout the sample.

The pure calcite powder that was used previously was extremely fine, so to ensure the lack of SHG signal seen was not due to the small particle size, larger crystals were grown. When the larger pure calcite crystals were imaged, some small regions of SHG signal were detected. However, the signal was ~41× weaker than that seen in otoconia. The extremely weak SHG signal given from the calcite crystal is indicative that calcite cannot

be solely responsible for the intense SHG signal seen in otoconia. Again, it is possible that this low signal is being caused by impurities becoming trapped within the crystals during the growth procedure. Based on this conclusion, we then hypothesized that the proteins embedded within otoconia, particularly otolin, which has been described to have collagen-like structural properties, are responsible for the majority of SHG signal observed in otoconia (Lundberg et al. 2015). In addition, similar to collagen, otolin features a triple helix structure (Yang et al. 2011). Based on previous research, it is known that collagen intrinsically gives high SHG signal supporting the prediction that otolin may be causing the SHG signal in otoconia (Tokarz et al. 2015) (Mostaço-Guidolin et al. 2017).

Due to the fact that we could see signal using impure calcite mineral, we exposed it to 0.5 M EDTA and imaged over a period of approximately 90 minutes (Figure 8). The mean SHG intensity of the calcite mineral was calculated and plotted against the images over time (Figure 9). As shown in this figure, there was overall relatively no increase or decrease in the SHG signal, and the fluctuation in intensity was very minor. EDTA is known to degrade calcite, so initially, we hypothesized we would observe a decrease in signal (Walther, Blödow, Buder, et al. 2014). However, since it was determined that calcite itself is not responsible for the SHG signal in the impure sample, it makes sense that overall the signal would stay relatively stable. This further supports the finding that inclusions are responsible for the SHG signal seen in calcite mineral.

4.2 Study Objective 2: Determine the internal structural properties of otoconia and the changes that occur during degradation using SHG microscopy

When otoconia were imaged with SHG microscopy using linearly polarized light, it was observed that two lobe-like regions of the otoconia became visible (Figure 10). As the linear polarization was changed between eight different polarization angles, these lobes were observed to rotate with respect to the direction of the laser beam. This means that otoconia are polarization-dependent, which is a unique feature that only occurs with a few known structures, such as starch granules (Cisek et al. 2017).

This polarization-dependence facilitated the identification of otoconia from other structures such as collagen, present within the sample. This polarization-dependence also indicates that if proteins are responsible for emitting the SHG signal in otoconia that they are radially arranged extending from a central point, as shown in Figure 21. This is because previous research has shown that when SHG emitters are parallel with the laser beam, there will be strong signal, but as the emitters become more perpendicular to the beam, a loss in signal will result. By looking at Figure 11, the two visible lobes are always oriented the same way as the linear polarization, which is indicated by the arrows in the top right corner of each image. This finding is significant as previously, the arrangement of proteins within otoconia has been conflicting (Walther, Blödow, Bloching, et al. 2014). Previous research has suggested that otoconia are composed of a large central core of proteins (Deans et al. 2010). However, this research supports more recent studies that indicate the proteins extend from a central point, but would not be considered a core and instead a region of overlap (Walther, Blödow, Bloching, et al. 2014).

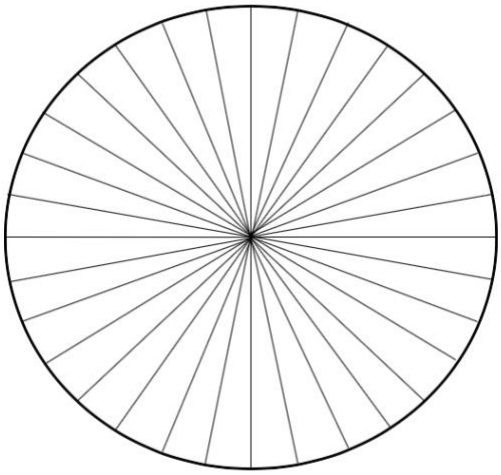

Figure 21: A model of the hypothesized arrangement of proteins causing the SHG signal in otoconia.

This finding is further supported by looking at otoconia using circularly polarized light (Figure 12). When circularly polarized light is used, it rotates as it passes through the sample and therefore is not going in one single direction like what happens when using linearly polarized light. For this reason, when using circularly polarized light, we see the entire crystal rather than just two lobes. However, we noticed that in each of the otoconia imaged using circularly polarized light; there was a small dark spot in the central region of each of the otoconia. This dark region or cancellation of signal has been previously described in other structures such as starch granules (Cisek et al. 2017). It has been determined that this effect can be caused by oppositely oriented SHG emitters that will cause a localized cancellation of signal, which is what we would expect if the proteins were extending from a central location oppositely of one another (Moreaux et al. 2000).

The last experiment performed was to expose otoconia to 0.5 M EDTA for a period of ~90 minutes. The mean SHG intensity was calculated and plotted against time after EDTA exposure. For all three otoconia, it was observed that SHG intensity increased over

time with exposure to EDTA (Figures 14, 15, & 17). Images of the otoconia were taken at each data point, and when comparing the first and last image of all three otoconia, the last image is visibly brighter (Figures 14, 16, & 18). Since EDTA is known to degrade calcium carbonate, it makes sense that we observed an increase in signal if proteins are the SHG emitters (Walther, Blödow, Buder, et al. 2014). As the calcite is degraded, it is likely exposing more proteins and, in turn causing an increase in SHG signal. This further supports our theory that proteins are the SHG emitters in otoconia.

4.3 Future Research and Applications

Several proposed ideas have been published to regenerate otoconia since they are unable to self-repair. These ideas include the re-expression of otoconial proteins and protecting or regenerating sensory hair cells which may be lost during otoconia degeneration such as generating hair cells from pluripotent stem cells (Lundberg et al. 2015) (Kang and Tusa 2013)(Merchant et al. 2000)(Koehler et al. 2013). SHG microscopy will provide insight to the structure of otoconia, particularly on the arrangement of protein allowing for more accurate development of artificial otoconia to treat vestibular pathologies. Despite these advancements, more research on otoconia structure is required in order to prevent otoconia degeneration to begin with.

By performing this study, it was determined that SHG microscopy is a promising imaging technique for investigating the internal structural properties of otoconia. Future studies using SHG microscopy should include imaging otoconia over time after exposure to ototoxic medications such as streptomycin antibiotics. Aminoglycoside antibiotics such as streptomycin are often unable to be used by practitioners due to the fact that they degrade

otoconia and therefore contribute to the development of vestibular pathologies (Selimoglu 2007).

By imaging otoconia with SHG their internal structure during antibiotic degradation can be observed to help visualize how their structure is altered. In addition to aminoglycoside antibiotics otoconia should be exposed to acidic solutions and observed using SHG microscopy. Previously, SEM was used to investigate how the surface structure of human otoconia changes with dissolution due to exposure to acidic conditions (using hydrochloric acid) (Walther, Blödow, Buder, et al. 2014). However, the internal structure of otoconia was not addressed in these studies and is needed to understand the results from aminoglycoside antibiotic structural alterations.

In addition to understanding more about the internal structure of otoconia these studies would allow us to create an automated measurement platform in order to objectively determine the stage of otoconia degeneration. Previous studies have determined levels of degradation by looking at surface morphology with SEM, but our technique will allow for an internal quantification as well (Walther, Wenzel, et al. 2014). By investigating the internal structural properties of otoconia researchers could apply this knowledge to try and find ways to prevent their degradation and design future therapies to treat vestibular pathologies.

LITERATURE CITED

Agrawal Y, Zuniga MG, Davalos-Bichara M, Schubert MC, Walston JD, Hughes J, Carey JP. 2012. Decline in semicircular canal and otolith function with age. Otol Neurotol Off Publ Am Otol Soc Am Neurotol Soc [and] Eur Acad Otol Neurotol. 33(5):832–839.

Atlantic Network for Injury Protection. 2003. Economic Burden of Unintentional Injury in Atlantic Canada. 17-21

Baconnier S, Lang S, Polomska M, Berkovic G, Mesh G. 2002. Calcite Microcrystals in the Pineal Gland of the Human Brain: First Physical and Chemical Studies. Bioelectromagnetics. 23:488–495.

Baloh R, Kerber K, Honrubia V. 2011. Baloh and Honrubia's Clinical Neurophysiology of the Vestibular System 4th ed. New York (NY): Oxford University Press Inc.

Barral J-P, Croibier A, Barral J-P, Croibier A. 2009. Vestibularcochlear nerve. In: Manual Therapy of the Cranial Nerves. London (EN): Churchill Livingstone. p. 167–180.

Bauer K-D, Hingerl K. 2017. Bulk quadrupole contribution to second harmonic generation from classical oscillator model in silicon. Opt Express. 25 (22): 26567-26580.

Bisht M, Bist SS. 2011. Ototoxicity: the hidden menace. Indian J Otolaryngol Head Neck Surg. 63(3):255–259.

Brauer P. 2003. Human Embryology: The Ultimate USMLE Step 1 Review. 1st ed. Philadelphia: Hanley & Belfus, INC.

Bueno JM, Ávila FJ, and Pablo Artal. 2016. Second Harmonic Generation Microscopy: A Tool for Quantitative Analysis of Tissues. In: Microscopy and Analysis. London (EN): IntechOpen. p. 99-119.

Casale J, Agarwal A. 2019. Anatomy, Head and Neck, Ear Endolymph. Treasure Island, (FL): StatPearls Publishing.

Casale J, Gupta G. 2019. Physiology, Vestibular System. Treasure Island, FL: StatPearls Publishing.

Cianfrone G, Pentangelo D, Cianfrone F, Mazzei F, Turchetta R, Orlando M, Altissimi G. 2011. Pharmacological drugs inducing ototoxicity, vestibular symptoms and tinnitus: a reasoned and updated guide. Eur Rev Med Pharmacol Sci. 15:601–636.

Cisek R, Tokarz D, Kontenis L, Barzda V, Steup M. 2017. Polarimetric Second Harmonic Generation Microscopy: An Analytical Tool for Starch Bioengineering. Starch - Stärke. 70 (1-2): 1-15.

Dakin Christopher J., Rosenberg A. 2018. Gravity estimation and verticality perception. Handb Clin Neurol. 159:43–59.

Dakin Christopher J, Rosenberg A. 2018. Gravity estimation and verticality perception. In: Balance, Gait, and Falls. Philidelphia (NY): Elsevier. p. 43–59.

Deans MR, Peterson JM, Wong GW. 2010. Mammalian Otolin: A Multimeric Glycoprotein Specific to the Inner Ear that Interacts with Otoconial Matrix Protein Otoconin-90 and Cerebellin-1. PLoS One. 5(9):1-15.

Fasano A, Plotnik M. 2012. Neurologic aspects and falls. Clin Cases Miner Bone Metab.

9(1):17–20.
Fettiplace R. 2017. Hair Cell Transduction, Tuning, and Synaptic Transmission in the Mammalian Cochlea. Compr Physiol. 7(4):1197–1227.
Franken PA, Hill AE, Peters CW, Weinreich G. 1961. Generation of Optical Harmonics. Phys Rev Lett. 7(4):118–119.
Glover JC. 2004. Vestibular System. In: Encyclopedia of Neuroscience. Cambridge (MA): Academic Press. p. 127–132.
Hain TC. 2007. Cranial Nerve VIII: Vestibulocochlear System. Textbook of Clinical Neurology (3rd ed.). Philidelphia (NY). Elsevier. p. 199–215.
Hancı D, Ulusoy S, Bayar Muluk N, Cingi C. 2015. Do viral infections have a role in benign paroxysmal positional vertigo? Acta Otorhinolaryngol Belg. 11:211–218.
Harnisch J, Frische M, Borchers R, Eisenhauer A, Jordan A. 2000. Natural fluorinated organics in fluorite and rocks. Geophys Res Lett. 27(13):1883–1886.
Hopkins K. 2015. Deafness in cochlear and auditory nerve disorders. In: The Human Auditory System (Vol. 129). Philidelphia (NY). Elsevier. p. 479–494.
Hughes I, Thalmann I, Thalmann R, Ornitz DM. 2006. Mixing model systems: using zebrafish and mouse inner ear mutants and other organ systems to unravel the mystery of otoconial development. Brain Res. 1091(1):58–74.
Iwasaki S, Yamasoba T. 2015. Dizziness and Imbalance in the Elderly: Age-related Decline in the Vestibular System. Aging Dis. 6(1):38–47.
Jang YS, Hwang CH, Shin JY, Bae WY, Kim LS. 2006. Age-Related Changes on the Morphology of the Otoconia. Laryngoscope. 116(6):996–1001.
Johnson EG. 2009. Clinical management of a patient with chronic recurrent vertigo following a mild traumatic brain injury. Case Rep Med. 2009 (910596): 1-3.
Kang C, Tusa R. 2013. Vestibular Rehabilitation: Rationale and Indications. Semin Neurol. 33:276–285.
Kao WTK, Parnes LS, Chole RA. 2017. Otoconia and otolithic membrane fragments within the posterior semicircular canal in benign paroxysmal positional vertigo. Laryngoscope. 127(3):709–714.
Kniep R, Zahn D, Wulfes J, Walther LE. 2017. The sense of balance in humans: Structural features of otoconia and their response to linear acceleration. PLoS One. 12(4):e0175769.
Koehler KR, Mikosz AM, Molosh AI, Patel D, Hashino E. 2013. Generation of inner ear sensory epithelia from pluripotent stem cells in 3D culture. Nature. 500(7461):217–221.
Kourosh P. 2014. Benign Paroxysmal Positional Vertigo: An Integrated Perspective. Adv Otolaryngol. 2014: 792635 (1-15).
Lim DJ. 1973. Formation and Fate of the Otoconia: Scanning and Transmission Electron Microscopy. Ann Otol Rhinol Laryngol. 82(1):23–35.
Lins U, Farina M, Kurc M, Riordan G, Thalmann R, Thalmann I, Kachar B. 2000. The Otoconia of the Guinea Pig Utricle: Internal Structure, Surface Exposure, and Interactions with the Filament Matrix. J Struct Biol. 131(1):67–78.
Lu W, Zhou D, Freeman JJ, Thalmann I, Ornitz DM, Thalmann R. 2010. In vitro effects of recombinant otoconin 90 upon calcite crystal growth. Significance of tertiary structure. Hear Res. 268(1–2):172-183.

Lundberg YW, Xu Y, Thiessen KD, Kramer KL. 2015. Mechanisms of otoconia and otolith development. Dev Dyn. 244(3):239–253.
Maga M. 2016. Postnatal Development of the Craniofacial Skeleton in Male C57BL/6J Mice. J Am Assoc Lab Anim Sci. 55(2):131–136.
Mason P. 2017. Medical Neurobiology. Oxford (EN): Oxford University Press.
Merchant SN, Tsuji K, Wall C, Velázquez-Villaseñor L, Glynn RJ, Rauch SD. 2000. Temporal Bone Studies of the Human Peripheral Vestibular System: 1. Normative Vestibular Hair Cell Data. Ann Otol Rhinol Laryngol. 109(5):3–13.
Mohler W, Millard AC, Campagnola PJ. 2003. Second harmonic generation imaging of endogenous structural proteins. Methods. 29(1):97–109.
Moreaux L, Sandre O, Blanchard-Desce M, Mertz J. 2000. Membrane imaging by simultaneous second-harmonic generation and two-photon microscopy: errata. Opt Lett. 25(9):678.
Mostaço-Guidolin L, Rosin NL, Hackett T-L. 2017. Imaging Collagen in Scar Tissue: Developments in Second Harmonic Generation Microscopy for Biomedical Applications. Int J Mol Sci. 18(8):1772 (2-23).
Murayama E, Herbomel P, Kawakami A, Takeda H, Nagasawa H. 2005. Otolith matrix proteins OMP-1 and Otolin-1 are necessary for normal otolith growth and their correct anchoring onto the sensory maculae. Mech Dev. 122(6):791–803.
Nova Scotia Government Health Promotion and Protection. 2007. Preventing Fall-Related Injuries Amoung Older Nova Scotians. 6–7.
Okeke M-U, Smith ST, Graf W. 2016. A Computational Model of Vestibular Fluid Response to Human Body Rotation. Am S Mech Eng. 3: 11-17.
Palmeri R, Kumar A. 2019. Benign Paroxysmal Positional Vertigo (BPPV). Treasure Island (FL): StatPearls Publishing.
Pantazis P, Maloney J, Wu D, Fraser SE. 2010. Second harmonic generating (SHG) nanoprobes for in vivo imaging. Proc Natl Acad Sci USA. 107(33):14535–14540.
Parnes L, Agrawal S, Atlas J. 2003. Diagnosis and management of benign paroxysmal positional vertigo (BPPV). CMAJ. 169:681–693.
Pearson SE, Taylor J, Hoare DJ, Patel P, Baguley DM. 2019. Exploring the Experiences of Cancer Patients With Chemotherapy-Induced Ototoxicity: Qualitative Study Using Online Health Care Forums. JMIR cancer. 5(1):e10883–e10883.
Purves D, Augustine G, Fitzpatrick D, Katz L, LaMantia A-S, McNamara J, Williams M. 2001. Neuroscience 2nd ed. Sutherland (MA): Oxford University Press.
Rabbitt RD. 2019. Semicircular canal biomechanics in health and disease. J Neurophysiol. 121(3):732–755.
Ray PC. 2010. Size and Shape Dependent Second Order Nonlinear Optical Properties of Nanomaterials and Their Application in Biological and Chemical Sensing. Chem Rev. 110(9):5332–5365.
Rehberg M, Krombach F, Pohl U, Dietzel S. 2011. Label-Free 3D Visualization of Cellular and Tissue Structures in Intact Muscle with Second and Third Harmonic Generation Microscopy. PLoS One. 6(11):e28237.
Roedder E. 1962. Ancient Fluids in Crystals. Sci Am. 207(4):38–47.
Rybak LP, Ramkumar V. 2007. Ototoxicity. Kidney Int. 72(8):931–935.
Samim M, Prent N, Dicenzo D, Stewart B, Barzda V. 2014. Second harmonic generation

polarization properties of myofilaments. J Biomed Opt. 19(5):1–6.
Selimoglu E. 2007. Aminoglycoside-Induced Ototoxicity. Curr Pharm Des. 13(1):119–126.
Sriram G, Sudhaharan T, Wright G. 2019. Multiphoton Microscopy for Noninvasive and Label-Free Imaging of Human Skin and Oral Mucosa Equivalents. Methods Mol Biol. 1-18
Stevenson A, Maurice W. 2011. Concise Oxford English Dictionary: Luxury Edition. Oxford University Press.
The Jackson Laboratory. 2009. Breeding Strategies for Maintaining Colonies of Laboratory Mice. 1–28.
Tokarz D, Cisek R, Golaraei A, Krouglov S, Navab R, Niu C, Sakashita S, Yasufuku K, Tsao M-S, Asa SL, et al. 2015. Tumor tissue characterization using polarization-sensitive second harmonic generation microscopy. SPIE. 9531: 5–30.
Walther LE, Blödow A, Bloching MB, Buder J, Carrillo-Cabrera W, Roseeva E, Borrmann H, Simon P, Kniep R. 2014. The Inner Structure of Human Otoconia. Otol Neurotol. 35(4): 686-694.
Walther LE, Blödow A, Buder J, Kniep R. 2014. Principles of Calcite Dissolution in Human and Artificial Otoconia. PLoS One. 9(7):1–9.
Walther LE, Wenzel A, Buder J, Bloching MB, Kniep R, Blödow A. 2014. Detection of human utricular otoconia degeneration in vital specimen and implications for benign paroxysmal positional vertigo. Eur Arch Oto-Rhino-Laryngology. 271(12):3133–3138.
Wang Y, Kowalski PE, Thalmann I, Ornitz DM, Mager DL, Thalmann R. 1998. Otoconin-90, the mammalian otoconial matrix protein, contains two domains of homology to secretory phospholipase A2; Proc Natl Acad Sci. 95(26):15345 – 15350.
Watson B, Salmoni A, Zecevic A. 2015. Falls in an acute care hospital as reported in the adverse event management system. J Hosp Adm. 4(4):84–91.
Wilson K, Rosenberg MW. 2002. The geographies of crisis: exploring accessibility to health care in Canada. Can Geogr / Le Géographe Can. 46(3):223–234.
Yang H, Zhao X, Xu Y, Wang L, He Q, Lundberg YW. 2011. Matrix Recruitment and Calcium Sequestration for Spatial Specific Otoconia Development. PLoS One. 6(5):e20498.